Plasma Cascade Instability

Vladimir N Litvinenko for CeC group

Yichao Jing, Jun Ma, Irina Petrushina, Igor Pinayev, Kai Shih, Gang Wang, Yuan Wu

Department of Physics and Astronomy, SBU

Collider-Accelerator Department, BNL

Center for Accelerator Science and Education

CASE
Center for Accelerator Science and Education

Content

- What is Plasma Cascade Instability (PCI)?
- How it occurs?
- How we can describe/simulate it?
- Experimental observations
- Controlling PCI
- Using PCI for CeC
- Conclusions

What is PCI?

- PCI is longitudinal micro-bunching instability occurring in charged beams propagating along a straight sections (no bending, no chicanes…)
- Initially we discovered this instability theoretically (in November/December 2017) in search of a broad-band instability to serve as an amplifier in Coherent electron Cooling (CeC) scheme, which does not require separation of electron and hadron beams
- We developed both the theory and simulations of the PCI to be used in our next CeC experiment
- Unexpectantly we discovered that is occurs in our CeC SRF accelerator at frequencies of 10s of THz
- We studied this instability experimentally in Summer of 2018 and demonstrated nearly 100% filamentation of the beam via PCI
- We developed methods to suppress PCI where it is harmful and use it where/when we need it

From first principles

- Short period perturbations of the longitudinal density in electron beam are described in co-moving frame by plasma oscillations

$$\frac{d^2\tilde{n}}{dt^2} + \omega_p^2 \tilde{n} = 0; \omega_p = c\sqrt{4\pi n_o r_c}$$

- If density n_o is constant, it is nothing else than boring than periodic oscillations with energy transferred back and forth from potential to kinetic
- Situation changes when density is modulated

$$\omega_p(t) = c\sqrt{4\pi n_o(t) r_c}$$

- and oscillations could become unstable..

Microwave instability

Broad-band instability described by Hill's equation

$$\frac{d^2\tilde{\eta}}{ds^2} + k_p^2(s)\tilde{\eta} = 0$$

or an harmonic

$$\tilde{\eta}_\omega = A(s)\cos\left(\omega\left(t - s/\mathrm{v}\right)\right);$$

$$\frac{d^2 A}{ds^2} + k_p^2(s) A = 0 \quad for\ any\ \omega!$$

No secret for this audience: depending on $k_p^2(s)$ "motion" can be stable or unstable

Stable

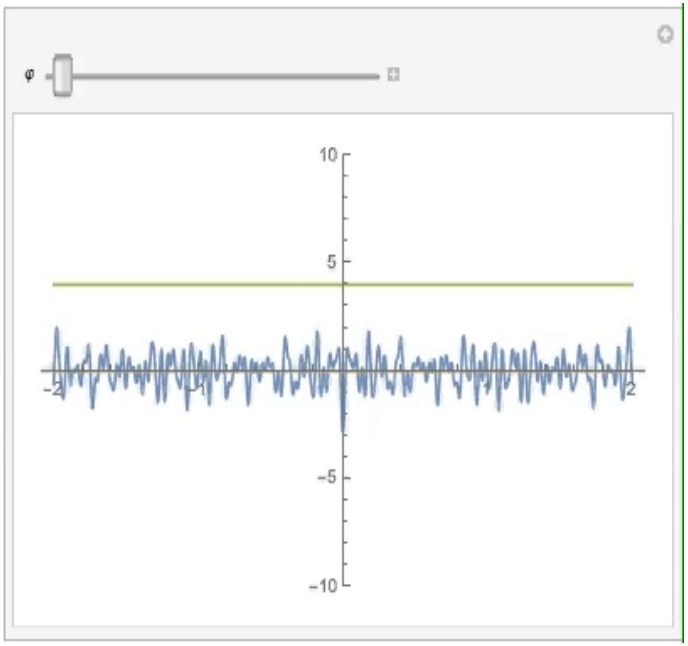

Unstable

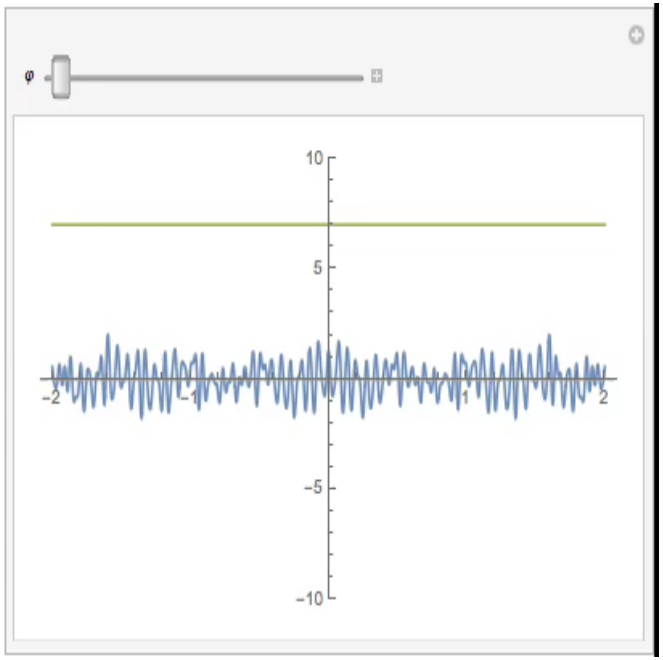

Index: Green – values of k_p, Blue – density modulation, Yellow – velocity modulation

Values are normalized for visibility

Parametric resonance –a playground swing

Simple rule: Change the length of the chains or momentum of inertia with twice the frequency of the swing.
Kids can do it and so can we…

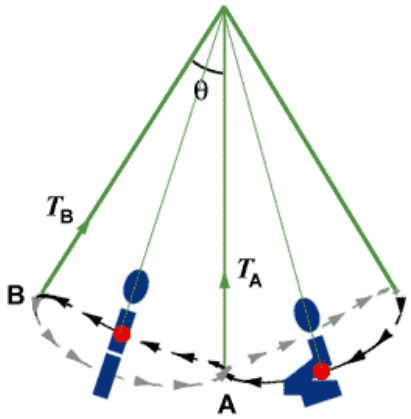

https://youtu.be/CzWelS_jiiQ

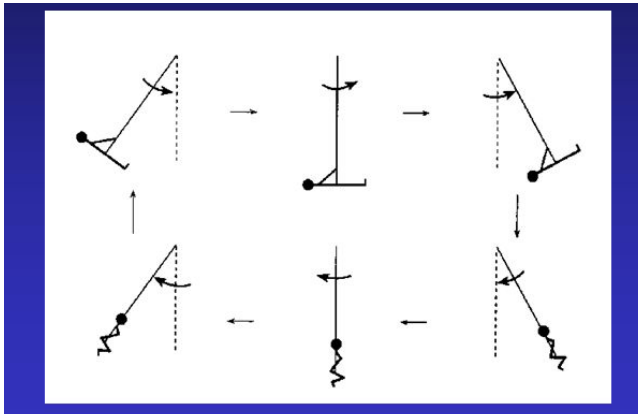


(a)


(b)

Simple picture: over focusing instability

$l > 2f$

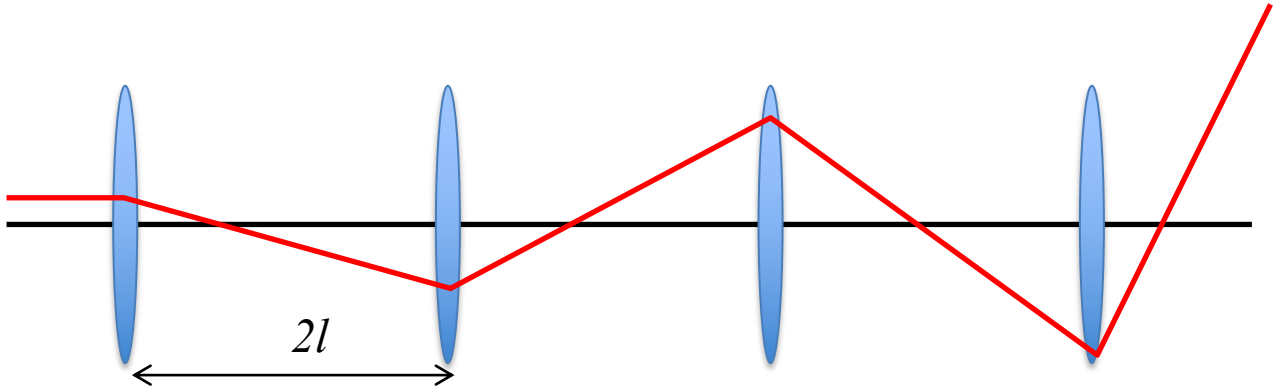

$$\mathbf{M} = \begin{bmatrix} m_{11} & m_{12} \\ m_{21} & m_{22} \end{bmatrix} = \begin{bmatrix} 1 & l \\ 0 & 1 \end{bmatrix}\begin{bmatrix} 1 & 0 \\ -f^{-1} & 1 \end{bmatrix}\begin{bmatrix} 1 & l \\ 0 & 1 \end{bmatrix} = \begin{bmatrix} 1-lf^{-1} & l\left(2-lf^{-1}\right) \\ -f^{-1} & 1-lf^{-1} \end{bmatrix};$$

$$\det \mathbf{M} = 1,\ \lambda_1\lambda_2 = 1$$

$$\lambda_{1,2} = m_{11} \mp \sqrt{m_{11}^2 - 1};$$

$$lf^{-1} > 2 \rightarrow m_{11} = 1 - lf^{-1} < -1;\quad m_{12} = l\left(2 - lf^{-1}\right) < 0;$$

$$\lambda_1 = m_{11} - \sqrt{m_{11}^2 - 1} < -1;\ \lambda_2 \equiv \lambda_1^{-1}.$$

$$\mathbf{M}Y_{1,2} = \lambda_{1,2}Y_{1,2};\ Y_{1,2} = \begin{bmatrix} \mathrm{w} \\ \pm \mathrm{w}^{-1} \end{bmatrix};\ \mathrm{w}^2 = \frac{-m_{12}}{\sqrt{m_{11}^2 - 1}} > 0;$$

$$X(n) = a_1\lambda_1^n Y_1 + a_2\lambda_1^{-n}Y_2;\ a_1 = \frac{1}{2}Y_2^T\mathbf{S}_{(2d)}X_o; a_2 = -\frac{1}{2}Y_1^T\mathbf{S}_{(2d)}X_o; X_o = \begin{bmatrix} x_o \\ x_o' \end{bmatrix};$$

$$X(n) = \begin{bmatrix} \frac{\lambda_1^n + \lambda_1^{-n}}{2} \\ \frac{\lambda_1^n - \lambda_1^{-n}}{2\mathrm{w}^2} \end{bmatrix} x_o + \begin{bmatrix} \mathrm{w}^2\frac{\lambda_1^n - \lambda_1^{-n}}{2} \\ \frac{\lambda_1^n + \lambda_1^{-n}}{2} \end{bmatrix} x_o'.$$

$$Y_2^T\mathbf{S}_{(2d)}Y_1 \equiv -Y_1^T\mathbf{S}_{(2d)}Y_2 = 2;$$

$$\mathbf{S}_{(2d)} = \begin{bmatrix} 0 & 1 \\ -1 & 0 \end{bmatrix}.$$

What is Plasma-Cascade Instability (PCI)?

How is it different from the previously known micro-bunching instability (MBI)?

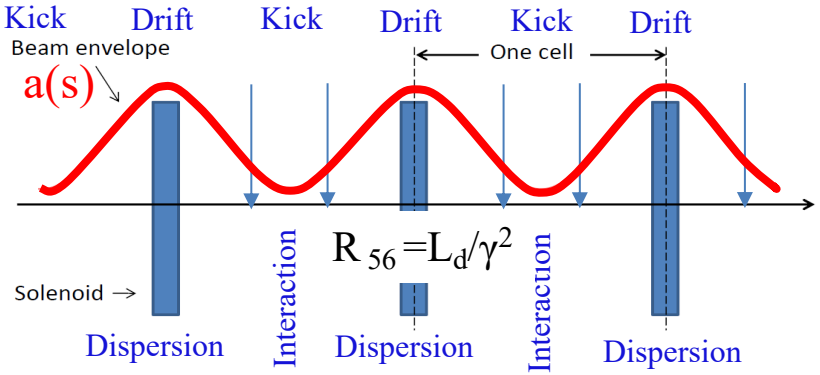

PCI

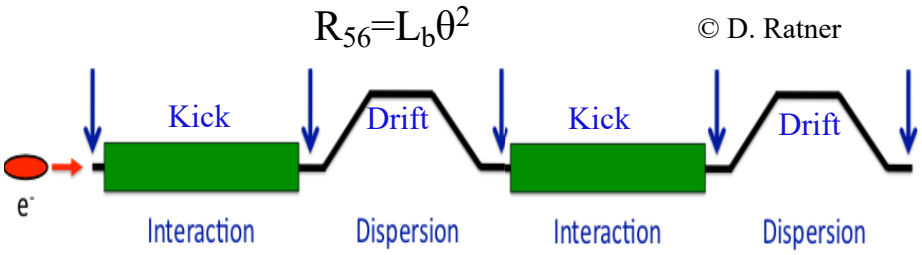

MBI

Modulate beam density by changing beam radius *a*:

Cold beam model

MBI: modulate effective mass (*s-mobility*) by bending beam trajectory (θ)

$$n_o(s) = \frac{I}{ev} \cdot \frac{1}{\pi a^2(s)}$$

$$n(t,s) = n_o(s) \cdot \{1 + \tilde{\eta}(s,t)\}$$

$$m_{eff} \approx m / (1 + \gamma^2\theta^2)$$

$$\frac{\partial n}{\partial t} + div(\vec{u}n) = 0;$$

$$\frac{d^2\tilde{\eta}}{ds^2} + k_p^2(s)\tilde{\eta} = 0;\ \tilde{\eta} = \tilde{\eta}(s,t);$$

$$k_p^2(s) = \frac{4\pi e^2 n_o(s)}{\gamma \cdot \gamma_z^2(s) \cdot mv^2};\ \gamma_z^2(s) = \frac{1}{1-\beta_z^2} \cong \frac{\gamma^2}{1+\gamma^2\theta^2(s)}$$

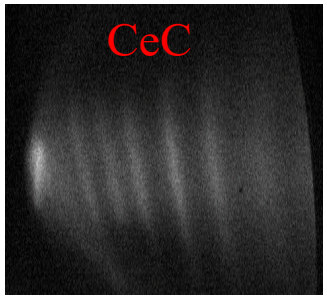

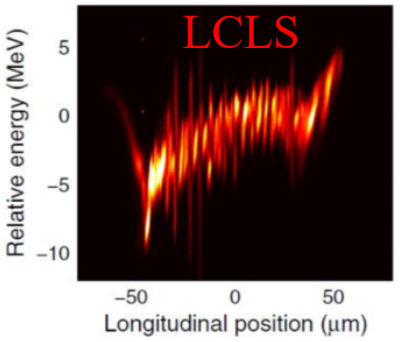

Plasma frequency does not dependent on the shape of modulation $\tilde{\eta}(t, s - vt)$

Detailed Theory of Plasma-Cascade Instability

- We developed a self-consistent theoretical approach describing Plasma Cascade Instability: details are in arxiv.org/abs/1802.08677
- This description is valid for high modulation frequencies/short wavelength modulation (period << a/γ). We separated equations for transverse and longitudinal motion
- Transverse motion is described by well-known envelope equation valid for K-V distribution

$$\hat{a}'' = k_{sc}^2 \hat{a}^{-1} + k_\beta^2 \hat{a}^{-3}; \quad \hat{s} = s / l$$

- Longitudinal equations are described by s-dependent plasma oscillations corrected by frequency dependent Landau damping

$$\tilde{n}_\omega = \tilde{\eta}_\omega \cdot \exp\left(s \frac{\omega}{\mathrm{v}} \frac{\sigma_\gamma}{\gamma^3} \right); \quad \frac{d^2 \tilde{n}_\omega}{ds^2} + 2k_{sc}^2 \left(\frac{a_o}{a(s)} \right)^2 \tilde{n}_\omega = 0$$

- For periodic system the dynamics is fully described by two dimensionless parameters representing space charge and emittance effects

$$k_{sc}^2 = \frac{2}{\beta^3 \gamma^3} \frac{I_o}{I_A} \frac{l^2}{a_o^{\,2}}; \quad k_\beta = \frac{\varepsilon l}{a_o^{\,2}} = \frac{l}{\beta^*}$$

where a_o is beam radius in the waist

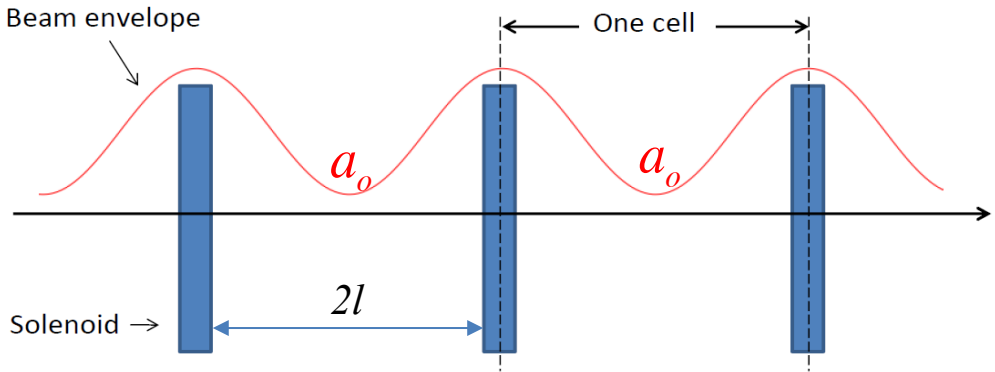

Separations of Hamiltonian

$$\frac{\partial}{\partial s} f(s,X) + \frac{\partial f}{\partial X} \cdot \left[S \frac{\partial}{\partial X} H(s,X) \right] = 0 \qquad X = (x, p_x, y, p_y, -t, E) \qquad \frac{d}{ds} X = S \frac{\partial}{\partial X} H(s,X)$$

$$S = \begin{pmatrix} 0 & 1 & 0 & 0 & 0 & 0 \\ -1 & 0 & 0 & 0 & 0 & 0 \\ 0 & 0 & 0 & 1 & 0 & 0 \\ 0 & 0 & -1 & 0 & 0 & 0 \\ 0 & 0 & 0 & 0 & 0 & 1 \\ 0 & 0 & 0 & 0 & -1 & 0 \end{pmatrix}$$

$$H(s,X) = H_{\perp}(s, X_{\perp}) + H_{//}(s, X_{//})$$

$$X_{\perp} = (x, p_x, y, p_y) \qquad X_{//} = (t, E)$$

$$S^{(4d)} = \begin{pmatrix} 0 & -1 & 0 & 0 \\ 1 & 0 & 0 & 0 \\ 0 & 0 & 0 & -1 \\ 0 & 0 & 1 & 0 \end{pmatrix}$$

$$\frac{\partial f}{\partial X} \cdot \left[S \frac{\partial}{\partial X} H(s,X) \right] = \frac{\partial f}{\partial X_{\perp}} \cdot \left[S^{(4d)} \frac{\partial}{\partial X_{\perp}} H_{\perp}(s, X_{\perp}) \right] + \frac{\partial f}{\partial X_{//}} \cdot \left[S^{(2d)} \frac{\partial}{\partial X_{//}} H_{//}(s, X_{//}) \right]$$

$$S^{(2d)} = \begin{pmatrix} 0 & -1 \\ 1 & 0 \end{pmatrix}$$

$$f(s, X_{\perp}, X_{//}) = f_{\perp}(s, X_{\perp}) f_{//}(s, X_{//})$$

$$f_{//}^{-1}(s, X_{//}) \left\{ \frac{\partial}{\partial s} f_{//}(s, X_{//}) + \frac{\partial f_{//}(s, X_{//})}{\partial X_{//}} \cdot \left[S^{(2d)} \frac{\partial}{\partial X_{//}} H_{//}(s, X_{//}) \right] \right\} + f_{\perp}^{-1}(s, X_{\perp}) \left\{ \frac{\partial}{\partial s} f_{\perp}(s, X_{\perp}) + \frac{\partial f_{\perp}(s, X_{\perp})}{\partial X_{\perp}} \cdot \left[S^{(4d)} \frac{\partial}{\partial X_{\perp}} H_{\perp}(s, X_{\perp}) \right] \right\} = 0$$

Decoupled Vlasov equations

$$\frac{\partial}{\partial s} f_{//}(s, X_{//}) + \frac{\partial f_{//}(s, X_{//})}{\partial X_{//}} \cdot \left[S^{(2d)} \frac{\partial}{\partial X_{//}} H_{//}(s, X_{//}) \right] = 0$$

$$\frac{\partial}{\partial s} f_{\perp}(s, X_{\perp}) + \frac{\partial f_{\perp}(s, X_{\perp})}{\partial X_{\perp}} \cdot \left[S^{(4d)} \frac{\partial}{\partial X_{\perp}} H_{\perp}(s, X_{\perp}) \right] = 0$$

Envelope equation & solution

$$j_o = en_{lab}\mathrm{v} = \frac{I_o}{\pi a^2};\ n_{lab} = \frac{I_o}{\pi e \mathrm{v} a^2}$$

K-V distribution

$$f_\perp\left(x,y,x',y'\right) = f_o\delta\left(I_x + I_y - \varepsilon\right)$$

$$I_x = \frac{x^2}{w_x^2} + \left(w_x x' - w_x' x\right)^2 = inv;\ I_y = \frac{y^2}{w_y^2} + \left(w_y y' - w_y' y\right)^2 = inv;$$

$$f_\perp\left(x,y,x',y'\right) = f_o\delta\left(I_x + I_y - \varepsilon\right);\ a_x = a_y = a;\ \beta_x = \beta_y = \beta$$

$$\beta_{x,y} \equiv w_{x,y}^2;\ a_{x,y} = \sqrt{\varepsilon\beta_{x,y}}$$

$$\rho\left(x,y\right) = \iint f_\perp dx'dy' = \left\{ \begin{array}{c} \frac{\pi f_o}{\beta}, r^2 \le a^2 \\ 0, r^2 > a^2 \end{array} \right\}$$

$$a"\left(s\right) + K\left(s\right)a\left(s\right) - \frac{2}{\beta^3\gamma^3}\frac{I_0}{I_A}\frac{1}{a\left(s\right)} - \frac{\varepsilon^2}{a\left(s\right)^3} = 0$$

In solenoid

$$K\left(s\right) = \left[\frac{eB_{sol}\left(z\right)}{2mc\beta\gamma}\right]^2$$

Between solenoids

$$\hat{a}'' = k_{sc}^2\hat{a}^{-1} + k_\beta^2\hat{a}^{-3}$$

$$k_{sc}^2 = \frac{2}{\beta^3\gamma^3}\frac{I_o}{I_A}\frac{l^2}{a_o^2};\ k_\beta = \frac{\varepsilon l}{a_o^2} = \left(\hat{\beta}^*\right)^{-1}$$

Longitudinal plasma oscillation

- Assumption – modulation wavelength in the co-moving frame is much smaller than transverse beam radius

$$\frac{\partial}{\partial t} f_{//}\left(z,v_z,t\right)+v_z\frac{\partial}{\partial z} f_{//}\left(z,v_z,t\right)+\dot{v}_z\frac{\partial}{\partial v_z} f_{//}\left(z,v_z,t\right)=0$$

$$f_{//}\left(z,v_z,t\right)=f_0\left(v_z\right)+f_1\left(z,v_z,t\right) \qquad \tilde{f}_1\left(k,v_z,t\right)\equiv\int_{-\infty}^{\infty} e^{-ikz} f_1\left(z,v_z,t\right)dz$$

$$f_0\left(v_z\right)=\frac{\rho_0}{\pi\sigma_z}\frac{1}{1+\frac{v_z^2}{\sigma_z^2}}$$

$$\tilde{E}_z\left(k,t\right)=\frac{ie}{k\varepsilon_0 S\left(t\right)}\tilde{\rho}_1\left(k,t\right) \qquad \tilde{E}_z\left(k,t\right)\equiv\int_{-\infty}^{\infty} E_z\left(z,t\right)e^{-ikz}\,dz \qquad \tilde{\rho}_1\left(k,t\right)\equiv\int_{-\infty}^{\infty}\rho_1\left(z,t\right)e^{-ikz}\,dz$$

$$\frac{\partial}{\partial t}\tilde{f}_1\left(k,v_z,t\right)+v_z\int_{-\infty}^{\infty}\frac{\partial}{\partial z}\left[e^{-ikz} f_1\left(z,v_z,t\right)\right]dz+ikv_z\tilde{f}_1\left(k,v_z,t\right)-\frac{e}{m_e}\tilde{E}_z\left(k,t\right)\frac{\partial}{\partial v_z} f_0\left(v_z\right)=0$$

$$\frac{\partial}{\partial t}\left[e^{ikv_z t}\tilde{f}_1\left(k,v_z,t\right)\right]=\frac{e}{m_e}\tilde{E}_z\left(k,t\right)e^{ikv_z t}\frac{\partial}{\partial v_z} f_0\left(v_z\right)$$

Hills equation

$$\frac{d^2}{dt^2}\hat{n}\left(k,t\right)+\frac{e^2\rho_0}{\varepsilon_0 m_e S\left(t\right)}\hat{n}\left(k,t\right)=0$$

including Landau damping $\qquad \hat{n}\left(k,t\right)\equiv\tilde{\rho}_1\left(k,t\right)e^{|k|\sigma_z t}$

Periodic systems

- Systems with arbitrary focusing can be solved only numerically, but periodic system can be studied systematically

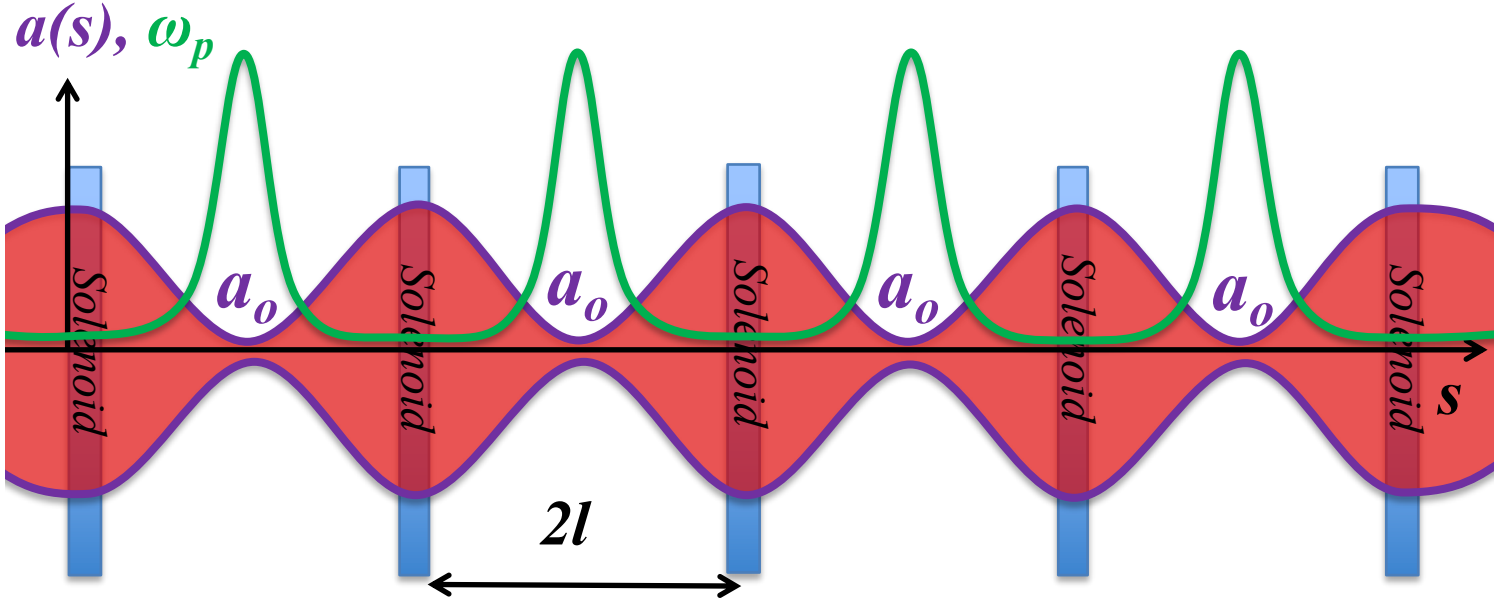

Dimensionless envelope equations

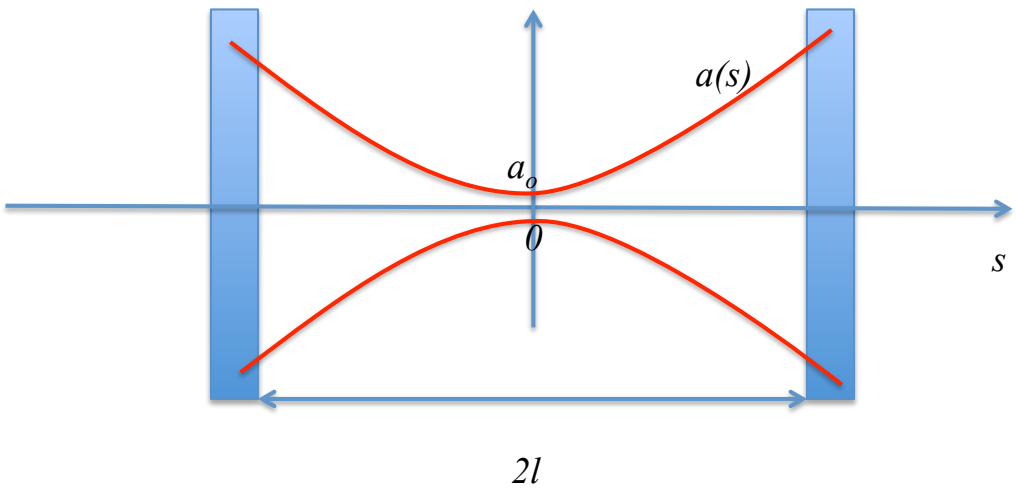

$$a'' - \frac{2}{\beta^3\gamma^3}\frac{I_o}{I_A}\frac{1}{a} - \frac{\varepsilon^2}{a^3} = 0;$$

$$h = \frac{a'^2}{2} - \frac{2}{\beta^3\gamma^3}\frac{I_o}{I_A}\ln\frac{a}{\varepsilon} + \frac{\varepsilon^2}{2a^2} = const;$$

$$a' = \sqrt{2\left(h - + \frac{2}{\beta^3\gamma^3}\frac{I_o}{I_A}\ln\frac{a}{\varepsilon} - \frac{\varepsilon^2}{2a^2}\right)}$$

$$\hat{s} = \frac{s}{l} \in \{-1,1\};\ \hat{a} = \frac{a}{a_o} \geq 1;\ \beta = \frac{\gamma a^2}{\varepsilon_n};\ \hat{\beta} = \frac{\beta}{l}$$

$$\hat{a}'' = k_{sc}^2\hat{a}^{-1} + k_\beta^2\hat{a}^{-3},\quad \hat{a}(0) = 1;\ \hat{a}'(0) = 0 \rightarrow \hat{a} = \hat{a}\left(\hat{s}, k_{sc}^2, k_\beta^2\right)$$

VL & Gang Wang

Final dimensionless equations

$$\hat{s} = \frac{s}{l} \in \{-1,1\};\ \hat{a} = \frac{a}{a_o} \geq 1;\ \beta = \frac{\gamma a^2}{\varepsilon_n};\ \hat{\beta} = \frac{\beta}{l}$$

$$\hat{a}'' = k_{sc}^2 \hat{a}^{-1} + k_\beta^2 \hat{a}^{-3},\quad \hat{a}(0) = 1;\ \hat{a}'(0) = 0 \rightarrow \hat{a} = \hat{a}\left(\hat{s}, k_{sc}^2, k_\beta^2\right)$$

$$\hat{n}'' + 2k_{sc}^2 \hat{a}(s)^{-2}\, \hat{n} = 0 \rightarrow \mathbf{D}(\hat{s}) = \mathbf{D}\left(\hat{s}, k_{sc}^2, \kappa^2\right) = \begin{bmatrix} 0 & 1 \\ -2k_{sc}^2 \cdot \hat{a}(s)^{-2} & 0 \end{bmatrix};$$

$$\mathbf{M}\left(0|\hat{s}\right) = \exp\left[\int_0^{\hat{s}} \mathbf{D}\left(\hat{s}, k_{sc}^2, \kappa^2\right) dz\right] = \mathbf{M}\left(\hat{s}, k_{sc}^2, \kappa^2\right);$$

$$\mathbf{M}(0|1) = \mathbf{M}\left(k_{sc}^2, \kappa^2\right);\ \mathbf{M}(-1|1) = \mathbf{M}\tilde{\mathbf{M}} = \begin{bmatrix} m_{11} & m_{12} \\ m_{21} & m_{11} \end{bmatrix};\ \lambda + \frac{1}{\lambda} = 2m_{11};\ \lambda_1 = 1/\lambda_2;$$

$$k_{sc}^2 = \frac{2}{\beta^3 \gamma^3} \frac{I_o}{I_A} \frac{l^2}{a_o^2};\ k_\beta = \frac{\varepsilon l}{a_o^2} = \left(\hat{\beta}^*\right)^{-1};\ f = \max\left[\mathrm{Re}(\lambda_{1,2})\right] = f\left(k_{sc}, k_\beta\right)$$

Growth rate per cell

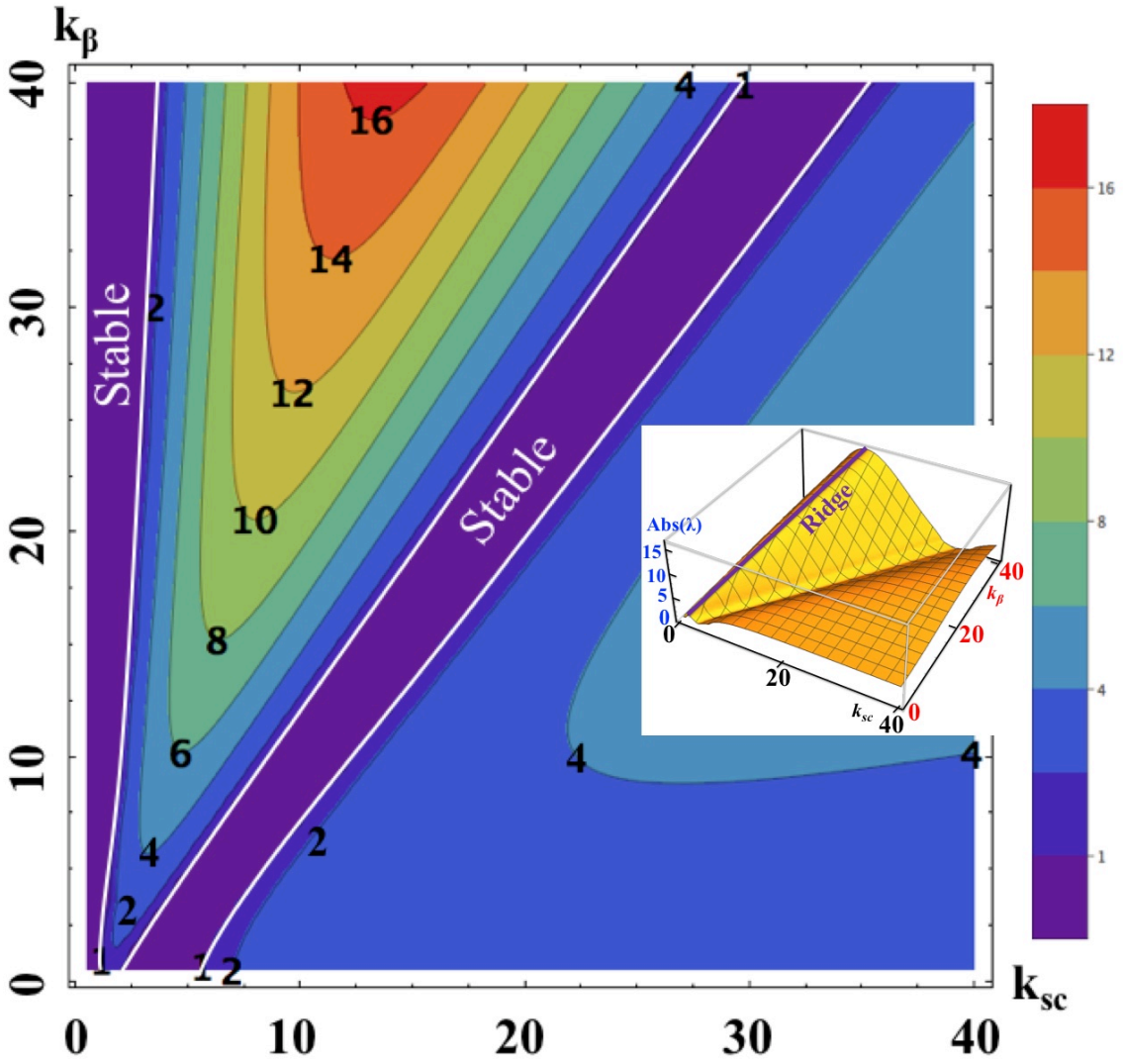

$$k_{sc}^2 = \frac{2}{\beta^3 \gamma^3} \frac{I_o}{I_A} \frac{l^2}{a_o^2}$$

$$k_\beta = \frac{\varepsilon l}{a_o^2} = \left(\hat{\beta}^*\right)^{-1}$$

$$f = \max[\mathrm{Re}(\lambda_{1,2})] = f\left(k_{sc}, k_\beta\right)$$

Simulation of Plasma-Cascade Instability

- SPACE code was modified to solve 3D beam dynamics of PCI self-consistently for a beam with a constant energy
- We had a good agreement between the theory and the SPACE 3D simulations for periodic systems and constant beam energy
- We comfortably predict performance of microbunching Plasma Cascade Amplifier (PCA) for CeC: either for CeC test experiment or for eRHIC energy
- We found a way of using a generic code Impact-T for simulating PCI in arbitrary accelerator (e.g. including acceleration and compression)

SPACE code simulations of microbunching PCA for CeC

14.5 MeV electrons

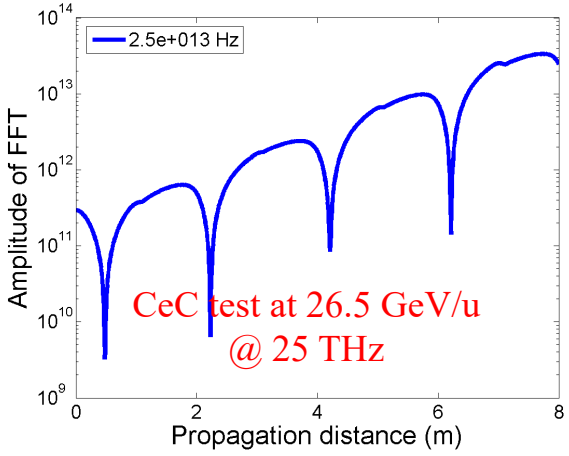

151 MeV electrons

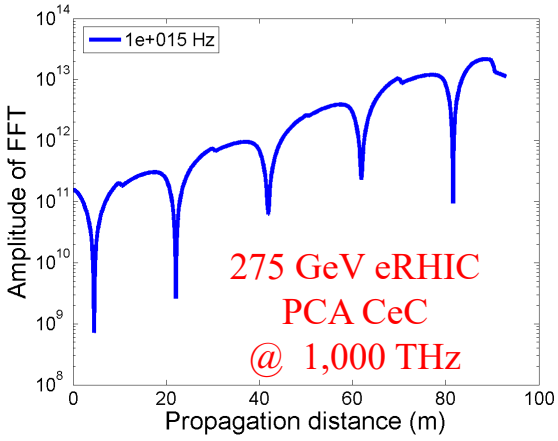

Evolution of a single ion imprint in 4-cell 8-meter Plasma Cascade Amplifier (PCA) using 3D SPACE code

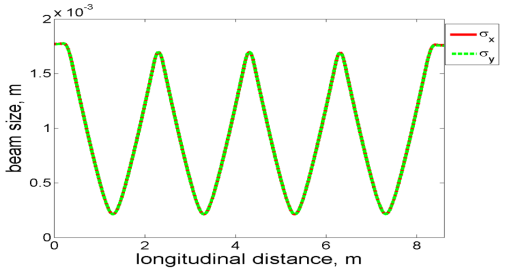

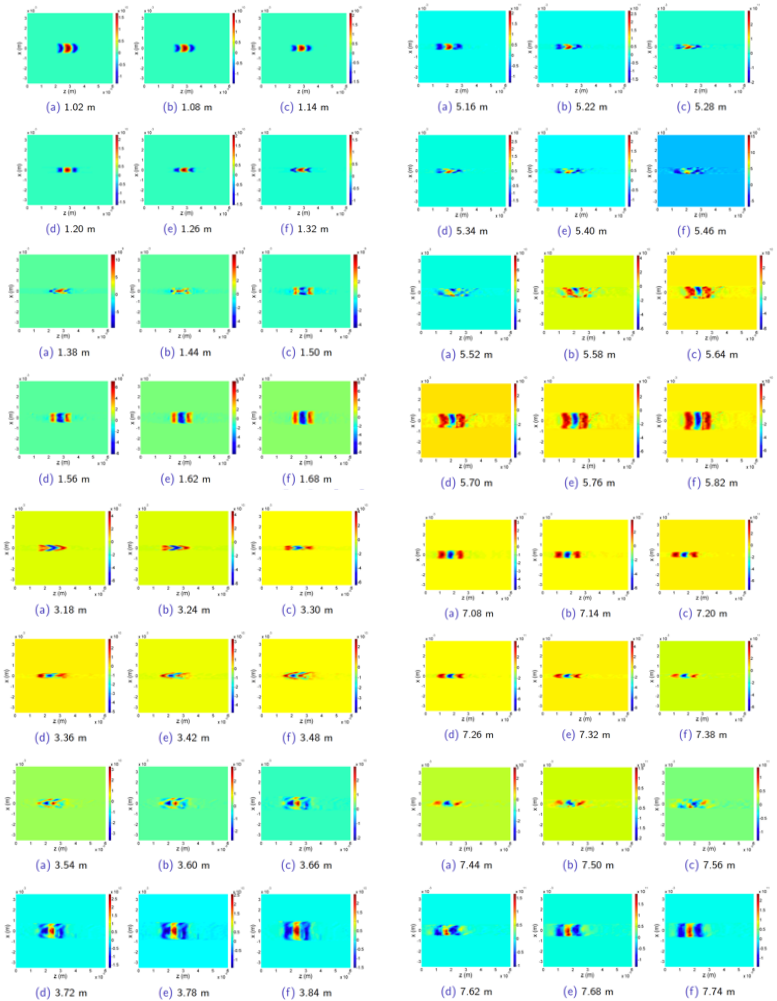

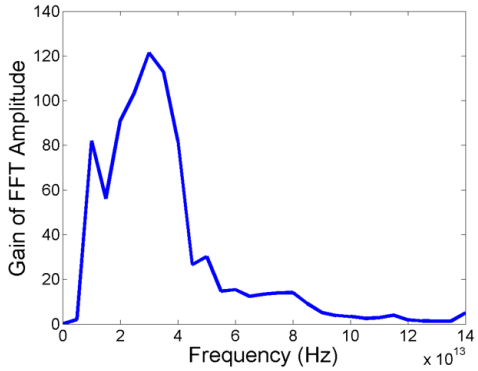

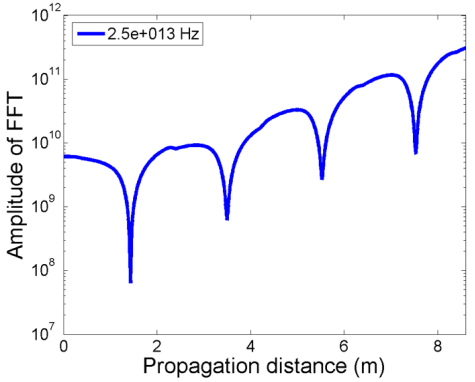

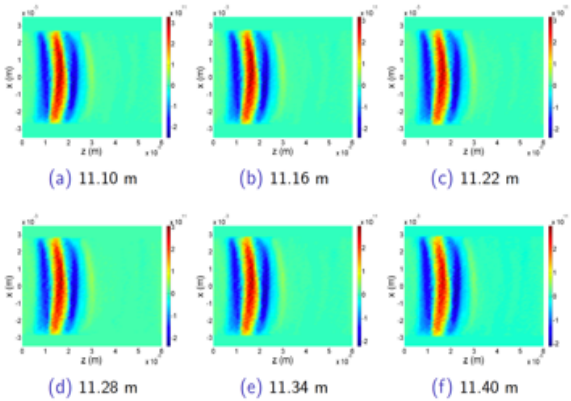

Evolution of a single ion imprint in the ACeC kicker.

3D effects are non-trivial: we clearly observe a number of eigen modes (Langmuir waves)

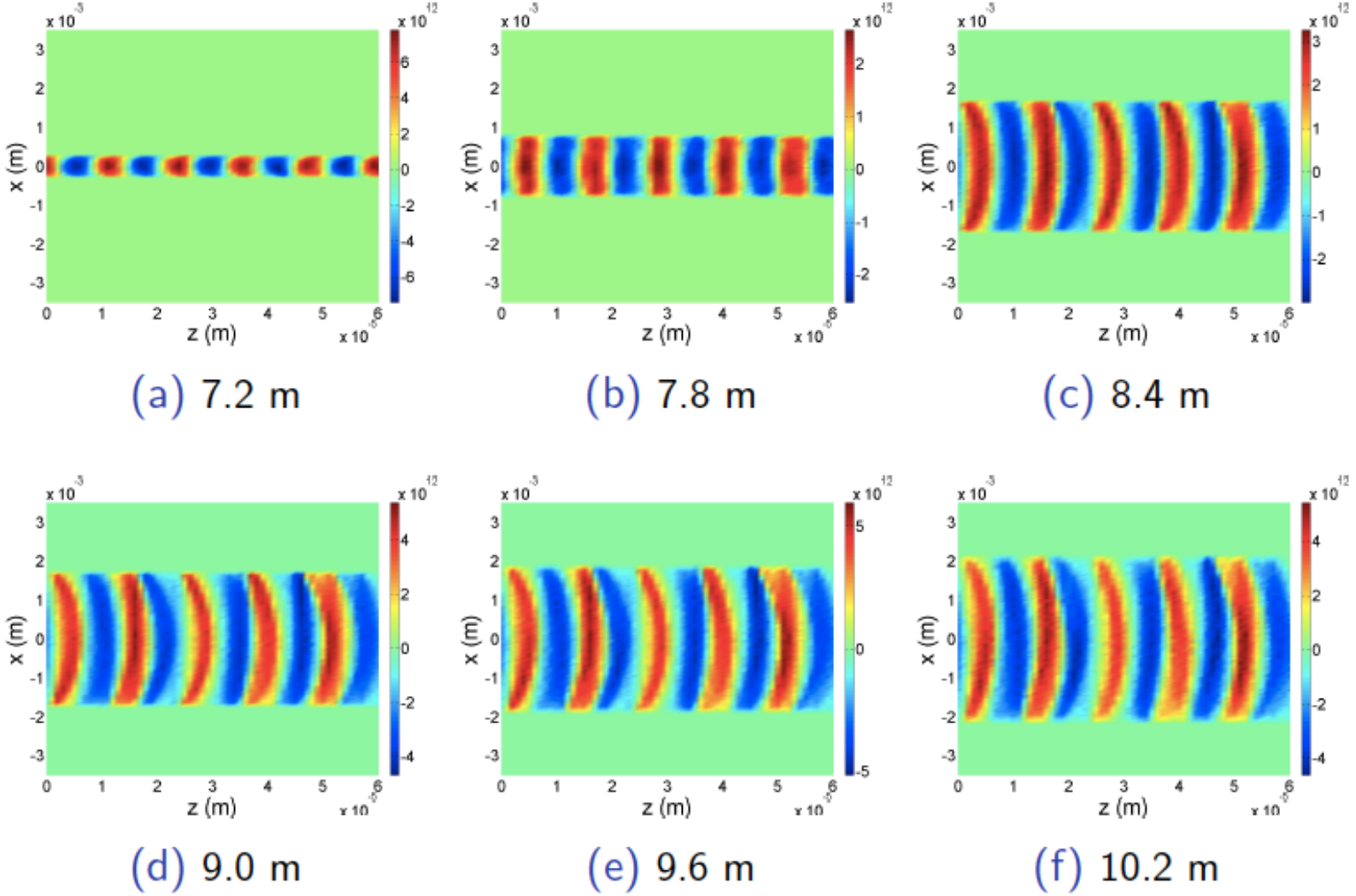

(a) 7.2 m (b) 7.8 m (c) 8.4 m

(d) 9.0 m (e) 9.6 m (f) 10.2 m

Experimental observation

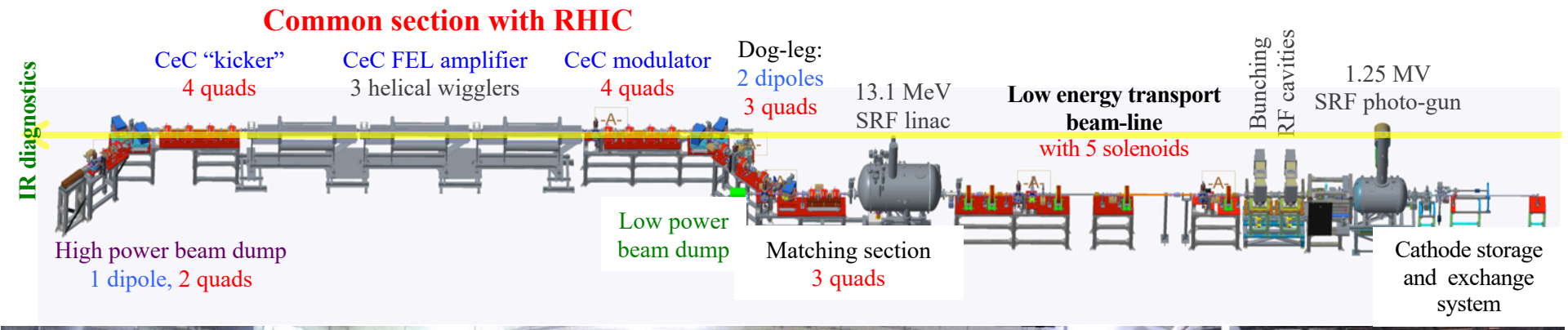

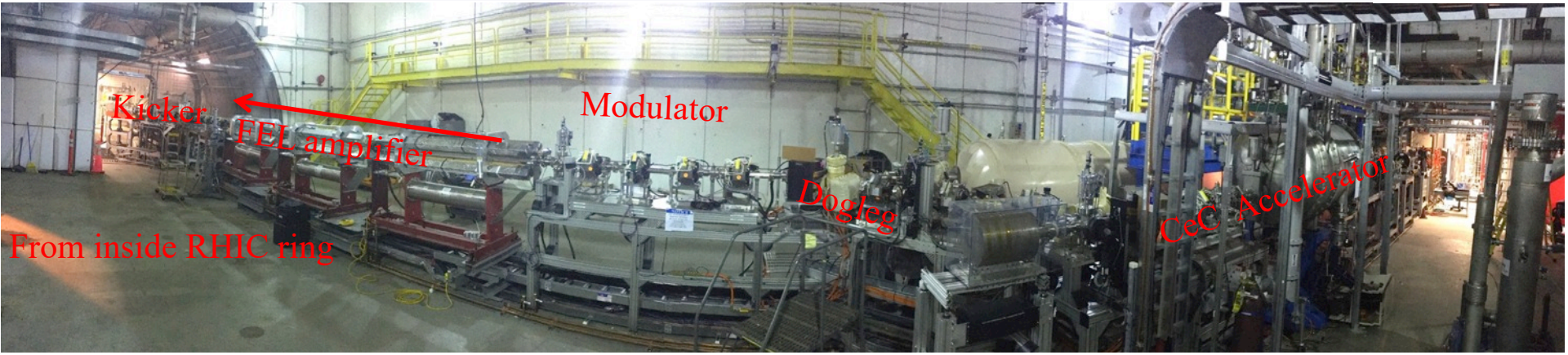

- First indication of PCI in CeC accelerator was observation of increased shot noise at frequencies of 10s of THz. It was deducted from 300-1000 fold increase in radiation power from FEL undulators and bending magnets. This radiation was from 14.5 MeV electron beam compressed to 50-100 A peak current
- All simulations using standard codes (elegant, Impact-T, Parmela, Astra,including space-charge, CSR and wakefields calculated by CST, Echo…) did not indicate any instability at high (e.g. THz) frequencies
- In August/September 2018 we conduced a dedicated experiment in the low energy beam transport having 6 solenoids and clearly observed saturated PCI

Run 18: compressed 14.56 MeV beam
7800 bunches, 0.6 nC/bunch

Nominal CeC setting
300x above shot noise

x 6.3 fold

1,900 x above shot noise

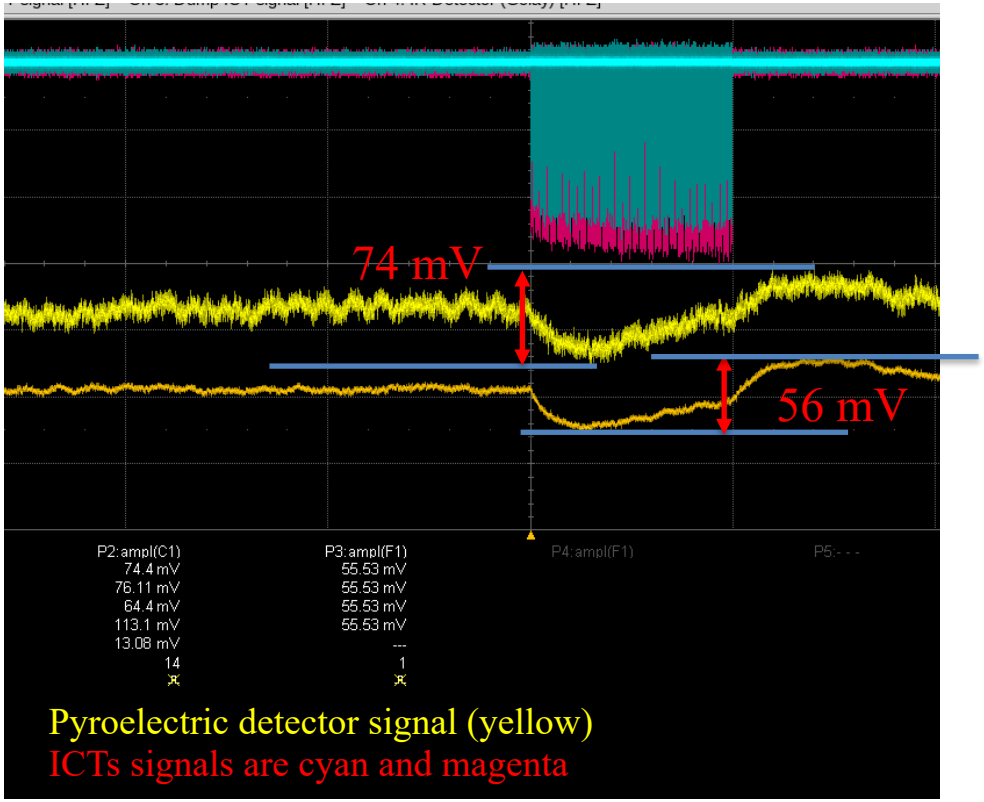

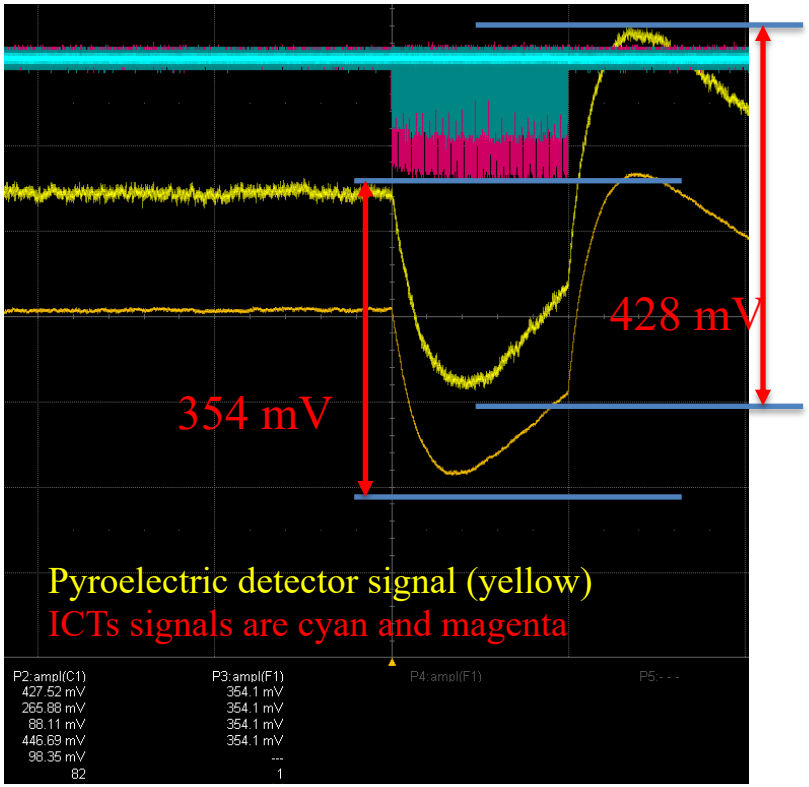

Turning linac & dogleg into e-beam psec time-resolved studies: $t \rightarrow E \rightarrow x$ transformer

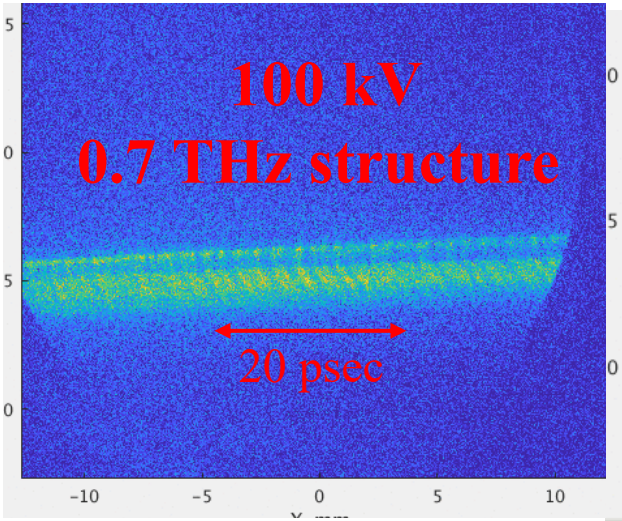

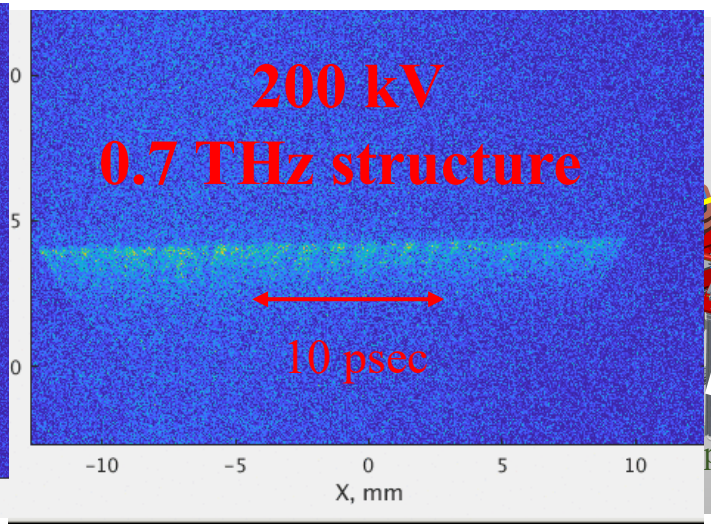

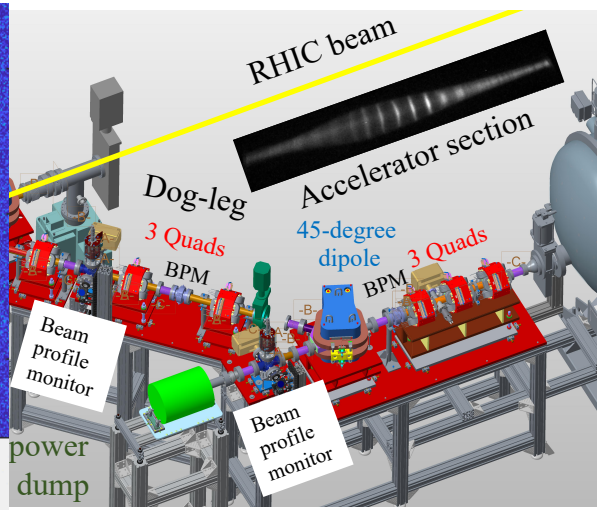

1.75 MeV uncompressed e-beam

- Operate SRF linac at low 100-200 kV voltage and zero-crossing to insert t-dependent chirp: $t \rightarrow E$
- Use D=1.36 m of the dogleg (quads off) as energy spectrometer: $E \rightarrow x$

Run 18: un-compressed beam with intentionally induced PCI

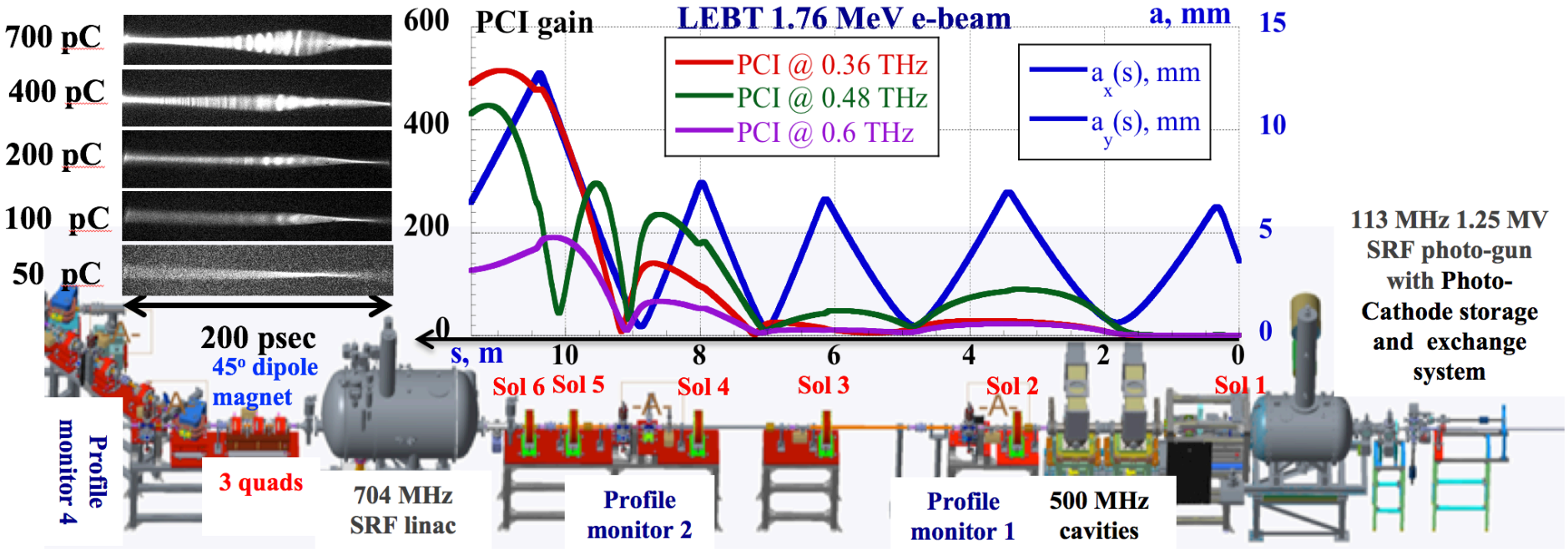

The CeC accelerator (right to left): the SRF electron gun, two bunching RF cavities, the LEBT line equipped with six solenoids and two profile monitors, followed by the 13.1 MeV SRF linac and a 45º bending magnet beam line (with three quadrupoles and a beam profile monitor).

The top graph shows simulated (by code SPACE) evolutions in the LEBT of the beam envelope (*a(s)*, blue line) and PCI gains at frequencies of 0.36 THz (red line), 0.48 THz (violet), and 0.6 THz (green). Simulations were done for 1.75 MeV (γ=3.443), 0.7 nC, 0.4 nsec electron bunch with 1 μm normalized slice emittance and 0.01% slice RMS energy spread.

Clip in the left-top corner shows time-resolved bunch profiles measured by the system for various charges in 400 psec electron bunch.

Run 18
un-compressed beam with intentionally induced PCI

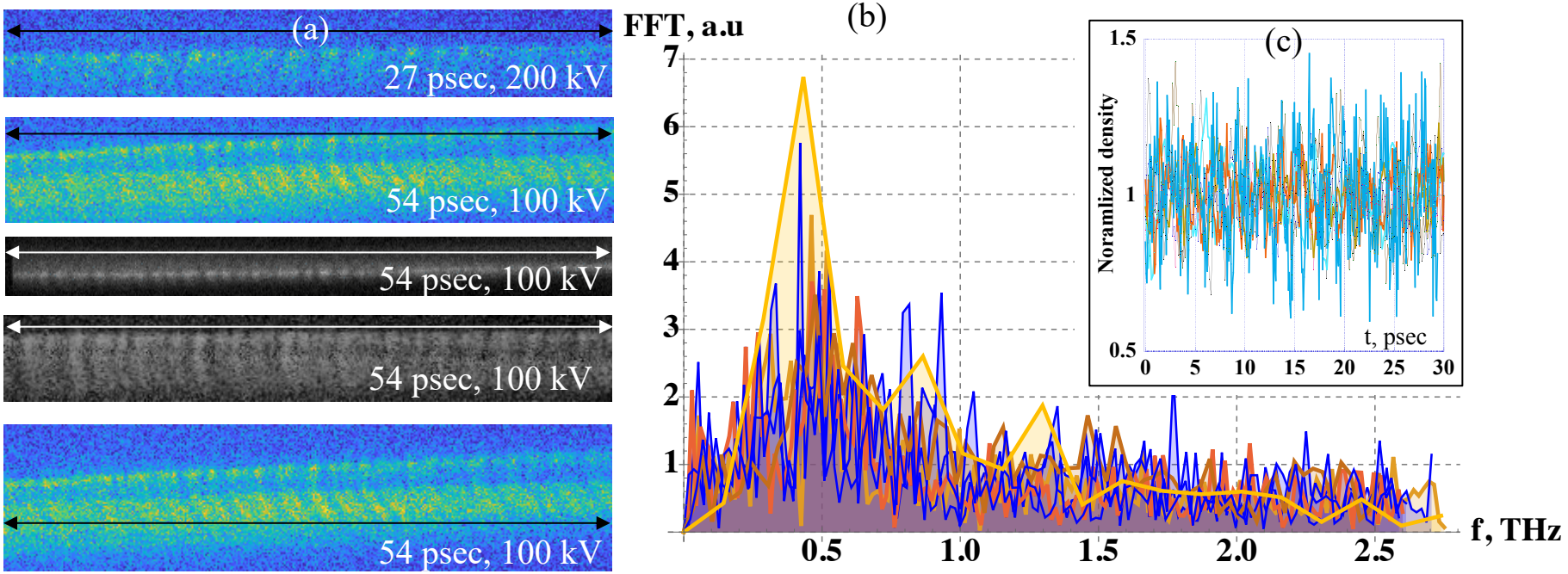

(a) Measured time profiles of 1.75 MeV electron bunches emerging from LEBT. Charge per bunch was from 0.45 nC to 0.7 nC

(b) Seven overlapping spectra of measured bunch density modulation and PCI spectrum simulated by SPACE (slightly elevated yellow line)

(c) Clip shows a 30-psec fragment of seven measured relative density modulations.

Simulation results of the PCI in CeC accelerator using Impact T

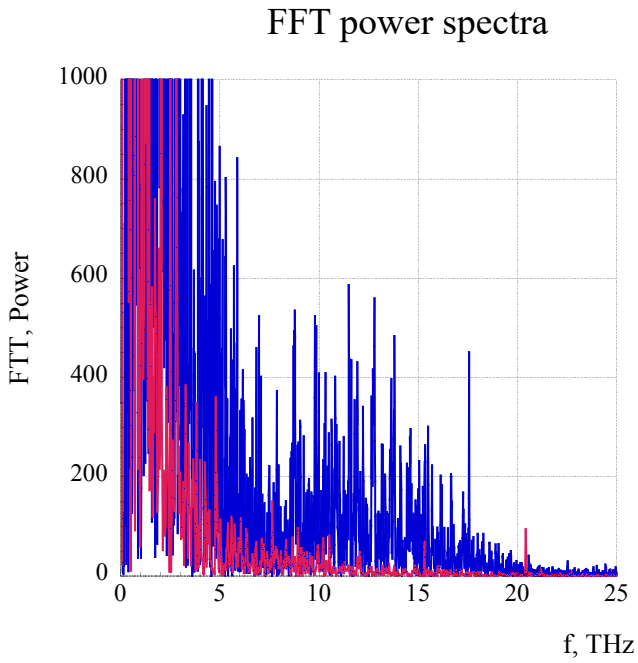

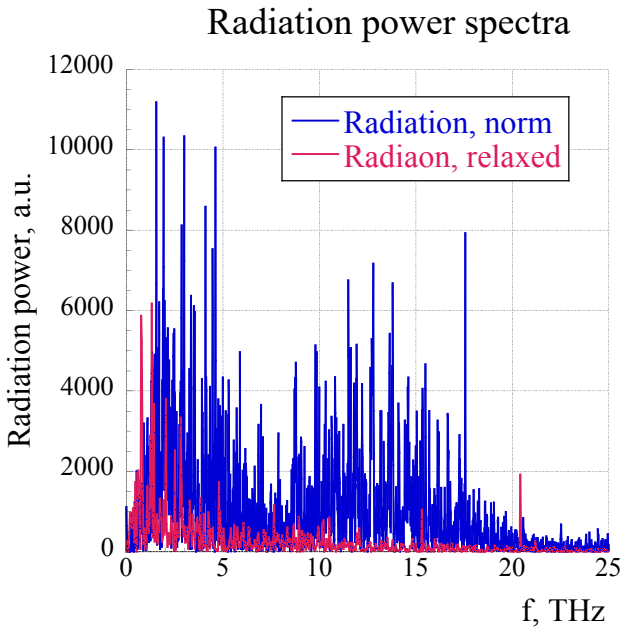

FTT and Radiation spectrum of the compressed 0.7 nC electron bunch profile at the exit of the SRF linac simulated by Impact-T. **Blue color lines** is for strong focusing lattice (used during RHIC Run 18) and **Red color lines** are for a new designed lattice of the CeC accelerator. Horizontal axis is the frequency measured in THz. The simulation was performed for 1.25 MV SRF gun voltage, standard bunching cavity voltages for 20-fold compression The relaxed LEBT lattice has following currents in six LEBT solenoids: 7.83 A, -2 A, 2 A, -2 A, 2 A, -2 A.

Reliable e-beam noise measurement system -Run 19

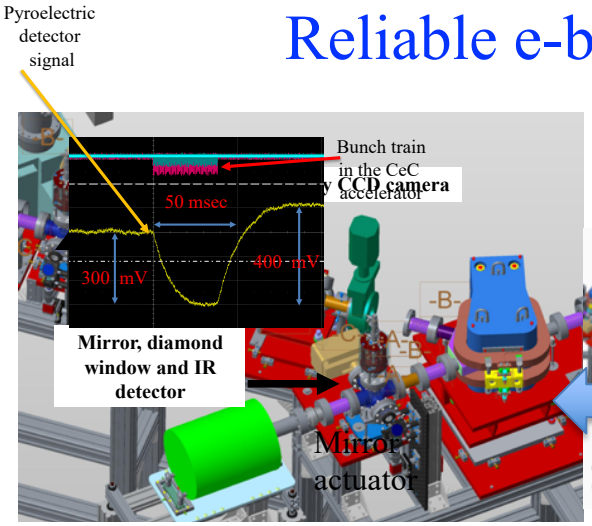

- **The goal of this short run was to control and reduce noise in electron beam below 100 times the shot noise baseline**
- **We operated CeC accelerator short 100 to 500 bunch trains repeated typically with 10 Hz and used IR detector, the lock-in amplifier and modulation-demodulation technique.**

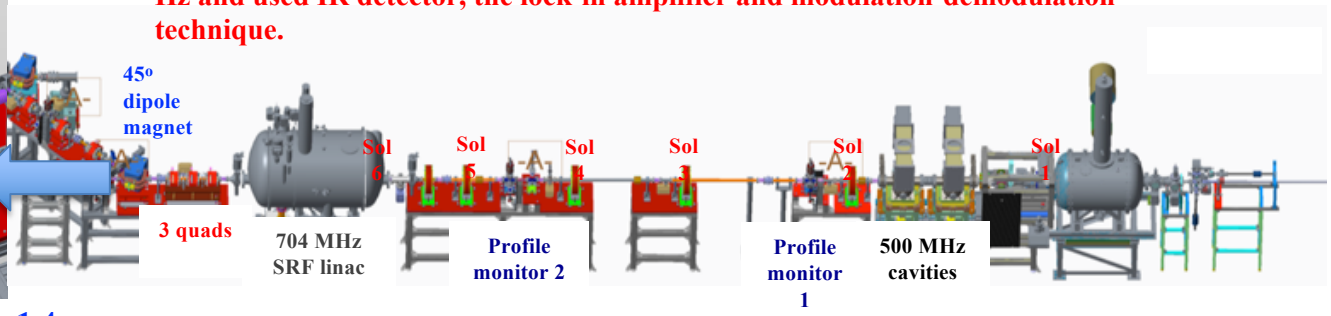

1" CVD diamond window with 1.4 mm x 1.4 mm metal mesh to stop GHz radiation from getting out

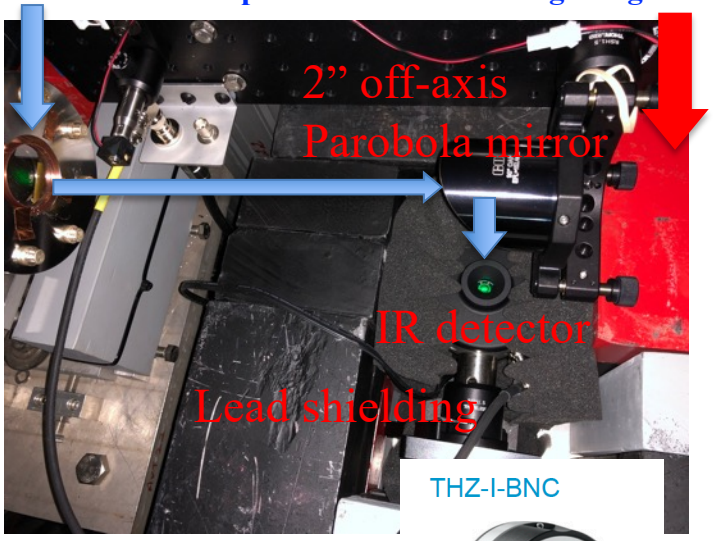

Pyroelectric detector
0.1 to 30 THz
(10 μm – 3 mm)

Response : 2.12 mV/nJ
Resolution of the system: ~0.1 nJ
Noise equivalent: 0.6 nW/Hz$^{1/2}$

We calibrated the lock-in amplifier output for such signal to be (4±0.4)·10^5 V/W. Spontaneous radiation power – e.g. that of e-beam with shot noise - reaching the insertable the 1" Cu mirror was calculated using Igor-Pro for beam bent in a measured magnetic field of the 45-degree dipole operated at 140 A. With metal mesh ~ 50% transparency we expected ~ 50 pW power reaching IR detector with typical 1.5 μA beam current and signal from locking amplifier signal ~ 20 μV

Igor-Pro simulation of the power distribution at the extraction mirror (right, red circle) and photon spectra for normal and 2.5 mrad beam entrance.

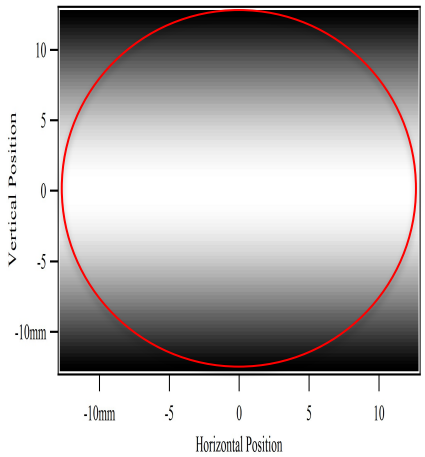

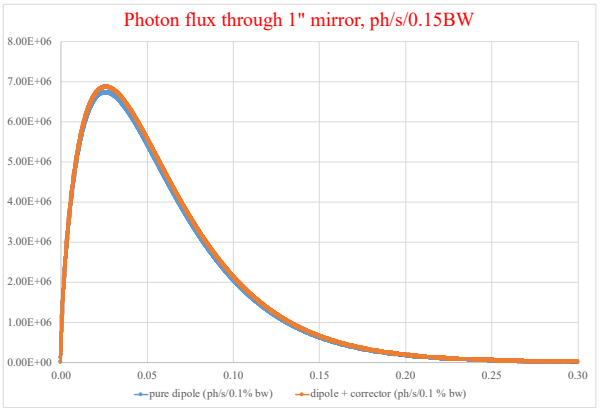

IR diagnostics 2
Pyroelectric detector
The range from 0.1 to 30 THz (10 μm – 3 mm)

THZ-I-BNC

Response : 2.12 mV/nJ
Resolution of the system: ~0.1 nJ
Noise equivalent: 0.6 nW/Hz$^{1/2}$

Pyroelectric detector signal

SPECIFICATIONS

	THZ5I-BL-BNC
MAX AVERAGE POWER	140 μW
EFFECTIVE APERTURE	5 mm Ø
INTEGRATED MODULE	Analog (BNC)
MEASUREMENT CAPABILITY	
Spectral Range [a]	
Frequency	0.1 - 30 THz
Wavelength	3000 - 10 μm
Max Measurable Power	140 μW
Noise Equivalent Power [b]	1.0 nW [1.0 x 10^{-9} W/(Hz)^{½}]
Rise Time (0-100%)	≤ 0.2s
Sensitivity (Typical) [b]	70 kV/W
Chopping Frequency	5 Hz (Required)

gentec-eo

Certificate #: 506449-171103
Model Number: THz5I-BL-BNC
Head Serial Number: 506449
Cal. Procedure: 100-1025
Customer Name:
Instrument ID:
Date of Calibration:
Calibration Due Date:

Calibration Data

Calibration					
Meaurement Parameter	Sensitivity		Into Load	Power	Rep.Rate
@ 633 nm	V/W	%	Ω	uw	Hz
Rv (P to P)	2.12E+05	± 2.1	NA	8.2	5
Rv (RMS)	6.91E+04	± 2.1	NA	8.2	5
					Hz

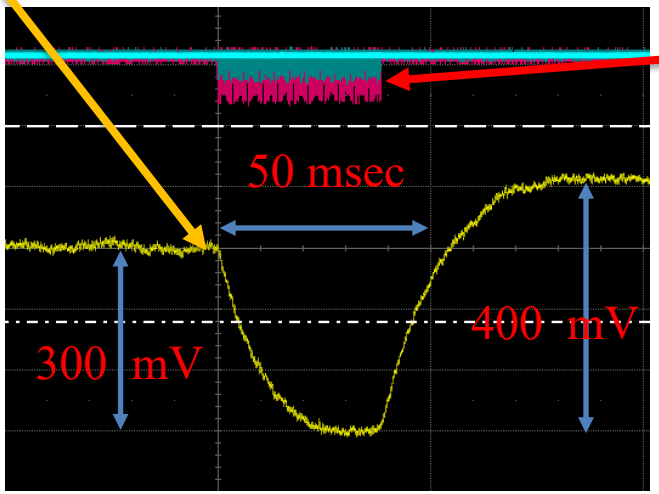

Bunch train in the CeC accelerator

Spontaneous synchrotron radiation

Theory

r	3.96E+01	cm
7/16 e^2/r	2.550827E-21	erg
dI/do	5.130532E-14	Erg/sterad
Density per electron	5.130532E-21	J/sterad
q	**1.5**	**nC**
Nb	**7800**	
Ne	7.30E+13	
Density per pulse	3.75E-07	J/sterad
Distance	0.7	m
Mirror Size (1" diameter)	25.4	mm
Area	506.71	mm^2
solid angle,	0.00103	rad^2
Integral	1.3	
Energy radiated into detector	0.504	nJ
Voltage	1.1	mV

$$\frac{dE_{rad}}{do} = \frac{7}{16}\frac{e^2}{\rho}\frac{\gamma^5}{\left(1+\gamma^2\theta^2\right)^{7/2}}\left[1+\frac{12}{7}\gamma^2\theta^2\right]$$

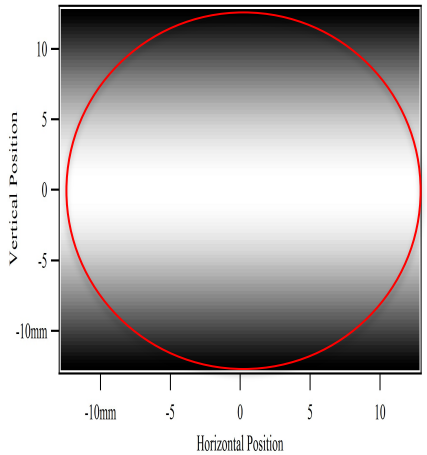

Complete agreement

Simulations

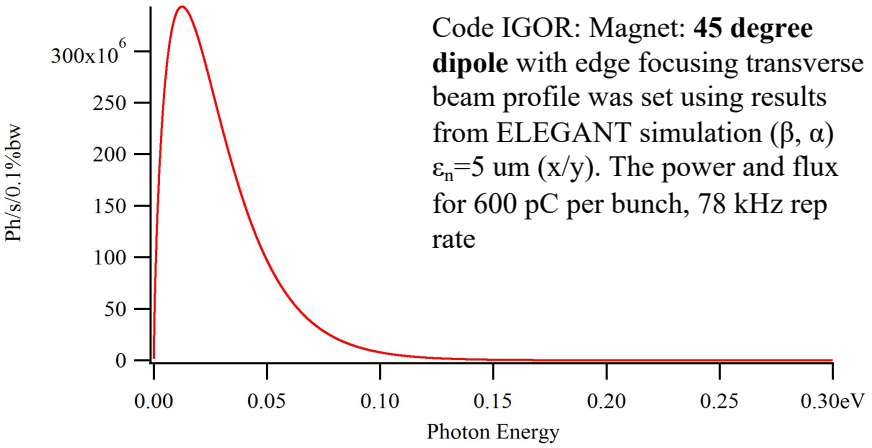

Code IGOR: Magnet: **45 degree dipole** with edge focusing transverse beam profile was set using results from ELEGANT simulation (β, α) ε_n=5 um (x/y). The power and flux for 600 pC per bunch, 78 kHz rep rate

0 12.5 25 37.5 THz

7,800 bunches, 1.5 nC

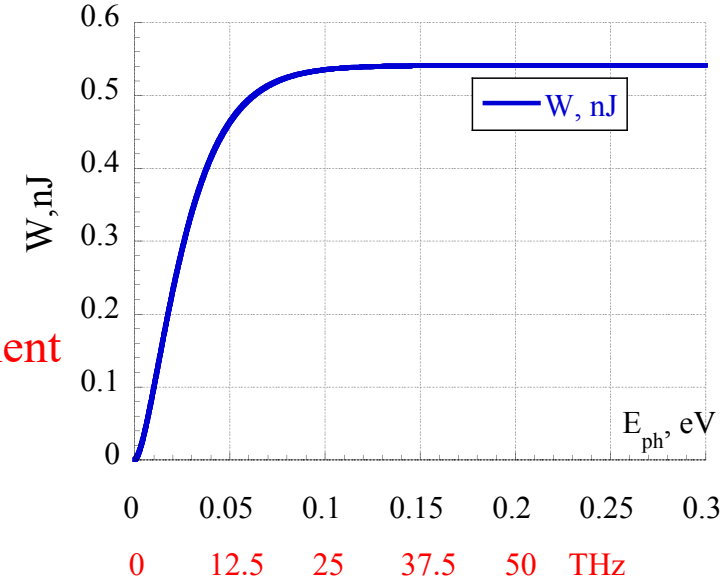

Controlling Plasma-Cascade Instability

Run 18 lattice and beam: 0.6 nC per bunch

Large signal of 2,500 V/A ~ 250-fold above base line.

Can be seen both on scope and measured easily

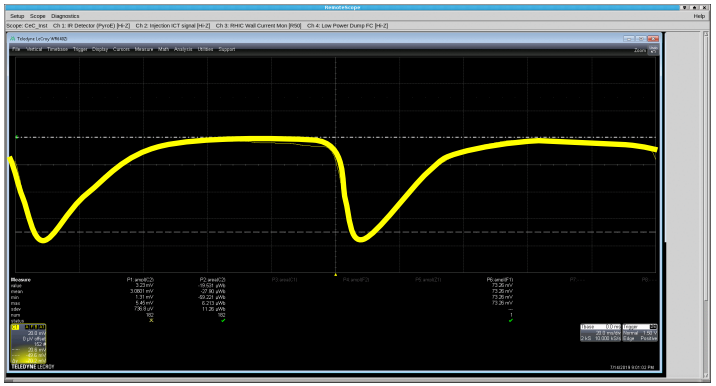

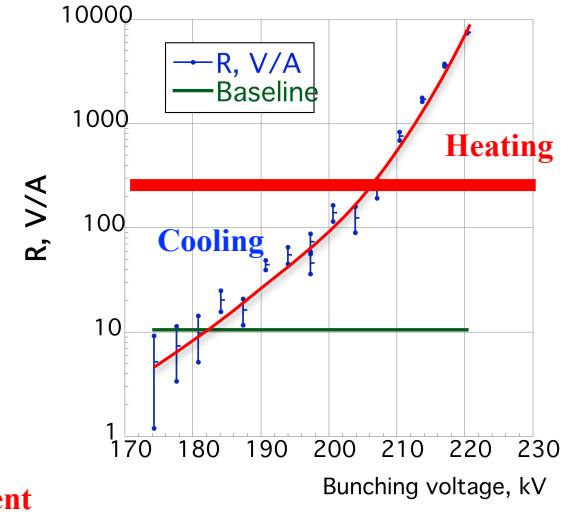

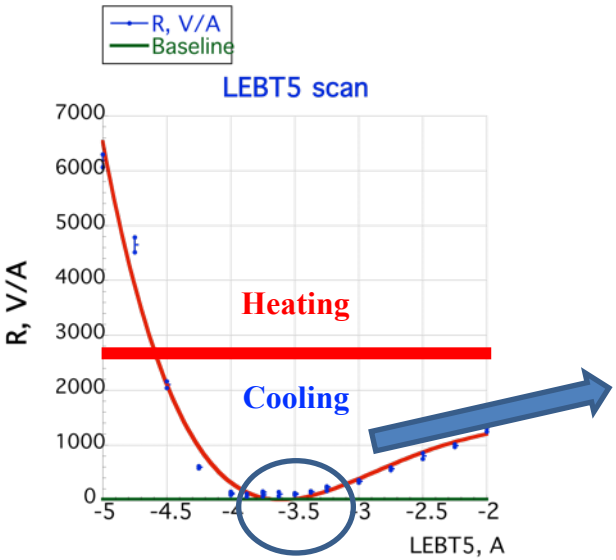

1.5 nC, 75 A peak current

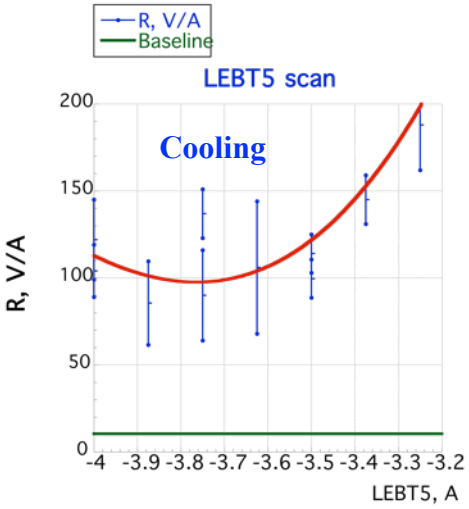

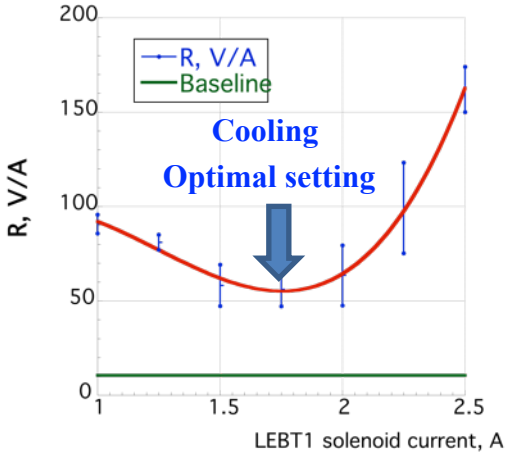

We demonstrated that with 75 A peak current we can reduce beam noise to acceptable level. It could be as low as 6-10 times above the baseline

RHIC Run 20 and beyond

when micro-bunching in the CeC accelerator is suppressed and necessary beam quality is established

Unchanged

Modulator

Kicker

4-cell PCA

Unchanged

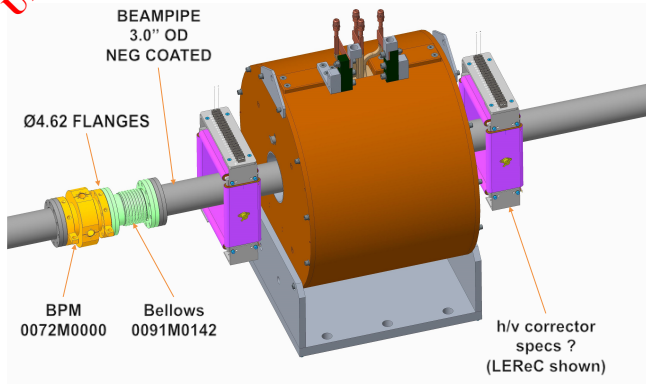

New equipment: solenoids are ordered and expected to arrive in Spring 2019

Design of CeC experiment
using Plasma-Cascade Amplifier (PCA)

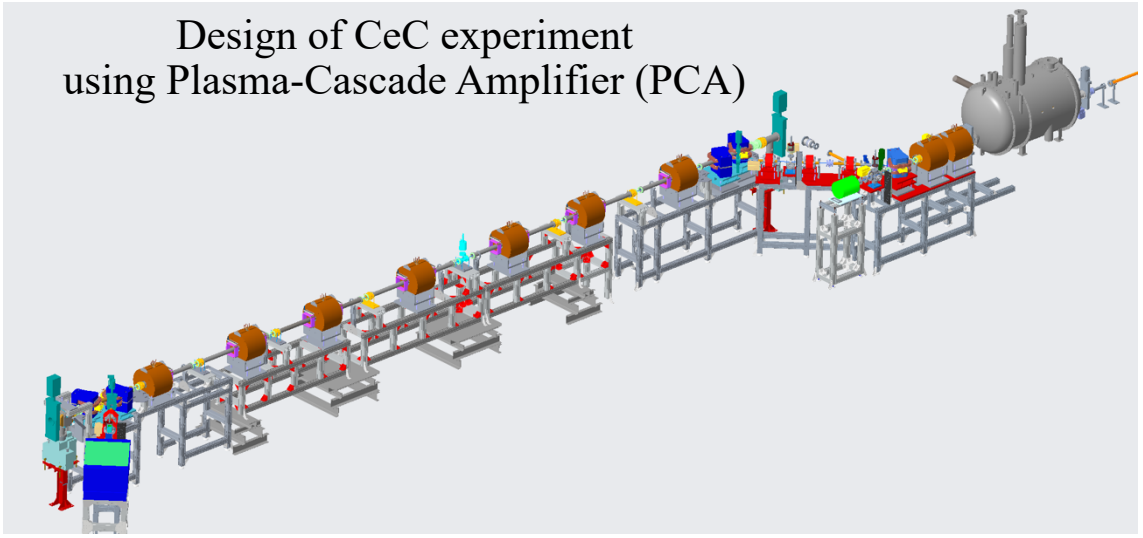

Predicted evolution of the 26.5 GeV/u ion bunch profile in RHIC

$$E_{fit}(z) = E_0 \frac{z}{\sigma_0} \cdot \left(1 + \frac{z^2}{\sigma_0^2}\right)^{-3/2}$$

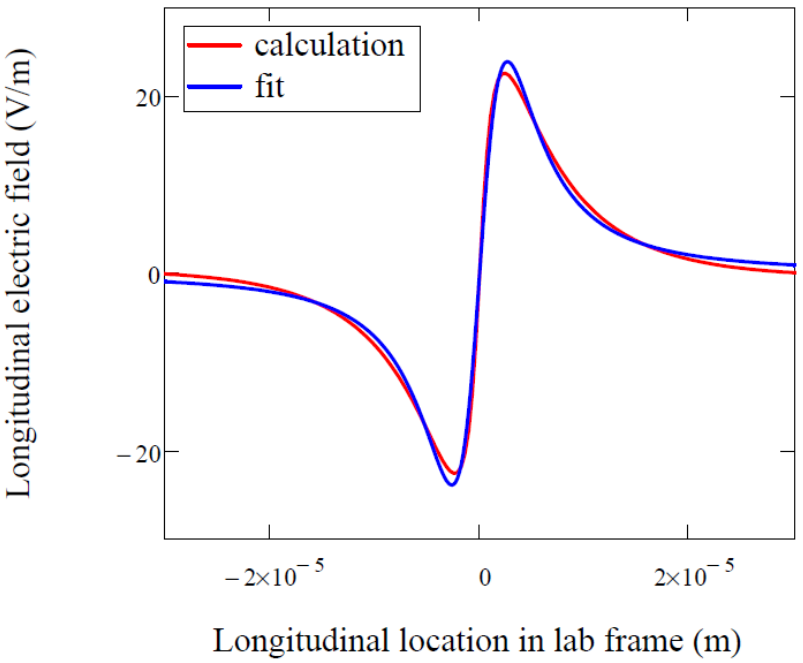

$$E_0 = 62.03 \ \ V/m$$

$$\sigma_0 = 3.75 \ \mu m$$

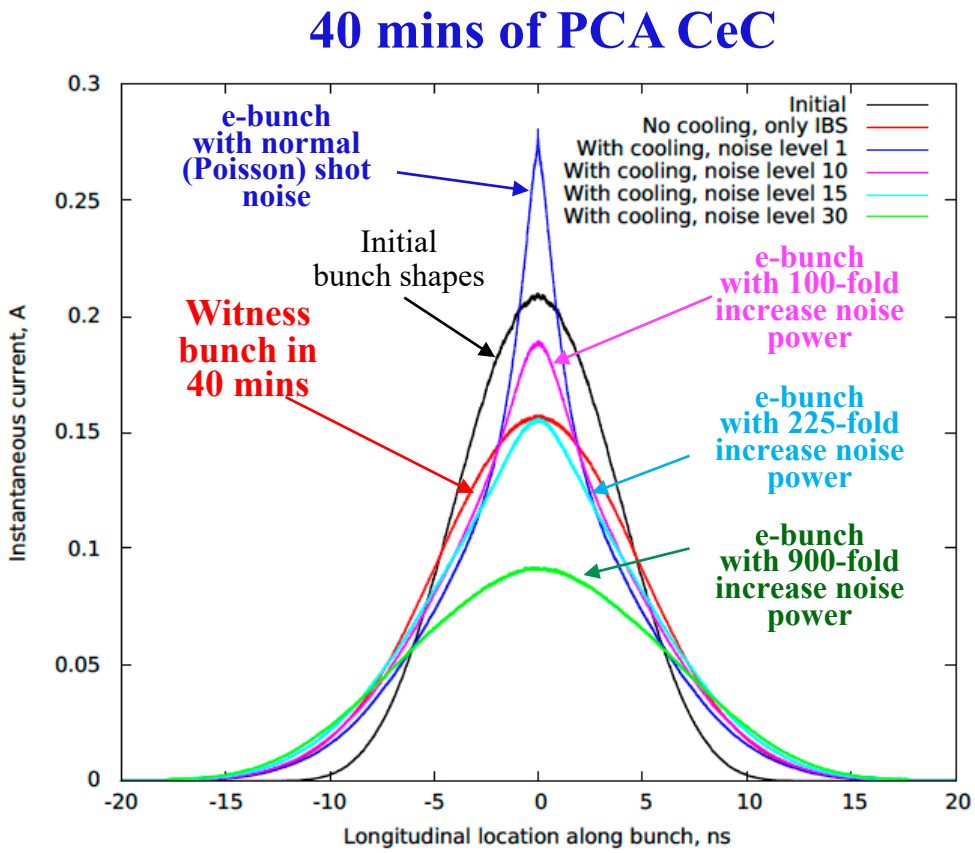

Simulated longitudinal profiles of 26.5 GeV ion bunches in RHIC. Black – initial profile, red – witness (non-interacting) bunch after 40 minutes. Profiles of interacting bunches after 40-minutes in PCA-based CeC for various levels of white noise amplitude in the electron beam: dark blue – nominal statistical shot noise, magenta – 10 fold, light blue – 15 fold and green – 30 fold - higher than the statistical level.

Cooling will occur if electron beam has micro-bunching with power (e.g. BM radiation power) less than 225-fold of spontaneous (shot noise) radiation

Conclusions

- As we had found, Plasma-cascade broad-band micro-bunching Instability (PCI) can be very harmful if you need a good quality electron beam. At the same time is can be explored for generating high power THZ and IR radiation, or as broad-band amplifier
- First we ran onto PCI while searching for a new broad-band amplifier for our CeC experiment. We developed both self-consistent theory and simulation tools for Plasma-Cascade Amplifier
- Few months later we ran into PCI in real experiment in form of excessive noise in the compressed electron beam. We studied PCI in low energy beam transport and developed simulation for an arbitrary linear accelerator.
- We are improving diagnostic and plan to suppress PCI instability the CeC accelerator and generate low-noise electron beams necessary for the CeC demonstration experiment
- Following this, we plan to continue with the PCA-based microbunching CeC experiment
- We acknowledge continuous support by C-AD management. Current CeC project is supported by Brookhaven Science Associates, LLC under Contract No. DE-AC02-98CH10886 with the U.S. Department of Energy and NSF Grant No. PHY-141525

Back-up slides

IR diagnostics 1

Golay cell: OPTOACOUSTIC DETECTOR

The wavelength range from 0.25μm to 6–8 mm

2. TECHNICAL DATA AND SPECIFICATIONS

- Diameter of entrance cone, mm: 11.0
- Diameter of entrance window, mm: 6.0
- Material of entrance window: ..... Synthetic diamond
- Operating wavelength range, μm: ..... 0.25 ÷ 4.0 & 6 ÷ 8000
- Recommended detected power, W, up to: ..... 1×10^{-5}
- Optimum modulation frequency, Hz: ..... 15 ± 5
- Noise-equivalent power @ 15Hz:
  - typical, $W/Hz^{1/2}$: ..... 1.4×10^{-10}
  - minimum, $W/Hz^{1/2}$: ..... 0.8×10^{-10}
- Optical responsivity @ 15Hz:
  - typical, V/W: ..... 1×10^{5}
  - maximum, V/W: ..... 1.5×10^{5}
- Response rate:
  - typical, ms: 35
  - minimum, ms: 25
- Detectivity (D*) at entrance cone aperture @ 15Hz:
  - typical, $cm\times Hz^{1/2}/W$: ..... 7.0×10^{9}
  - maximum, $cm\times Hz^{1/2}/W$: ..... 11.0×10^{9}
- Detectivity (D*) at entrance window aperture @ 15Hz:
  - typical, $cm\times Hz^{1/2}/W$: ..... 4.0×10^{9}
  - maximum, $cm\times Hz^{1/2}/W$: ..... 5.5×10^{9}

TYDEX®
RESEARCH & INDUSTRIAL OPTICS

CALIBRATION DATA

The calibration data are summarized in the table below:

Detector GC-1D	No. GC00060	
Power supply unit GC-PS/1	No. PS08005	
Window material	diamond	
Aperture of entrance cone	11 mm	
Aperture of entrance window	6 mm	
Reference frequency	5 Hz	10 Hz
Calibration power	1.17×10^{-6} W	1.17×10^{-6} W
Noise output at reference frequency	1.28×10^{-5} $V/Hz^{1/2}$	7.58×10^{-6} $V/Hz^{1/2}$
Optical responsivity at reference frequency	1.22×10^{5} V/W	1.01×10^{5} V/W
Response rate T_R (see Fig. 10)	38 ms	38 ms
Noise-equivalent power at reference frequency	1.05×10^{-10} $W/Hz^{1/2}$	7.52×10^{-11} $W/Hz^{1/2}$
Detectivity (D*) at entrance cone aperture	9.53×10^{9} $cmHz^{1/2}/W$	1.27×10^{10} $cmHz^{1/2}/W$
Detectivity (D*) at entrance window aperture	4.01×10^{9} $cmHz^{1/2}/W$	5.77×10^{9} $cmHz^{1/2}/W$

Response : 1.28 mV/nJ

Resolution of the system: ~0.2 nJ

Noise equivalent: 0.1 $nW/Hz^{1/2}$

Only if necessary – use filters (easy) or monochromator (need to move the box)

THz Band Pass Filters

THz Band Pass Filters are designed to transmit radiation in the wavelength range 20-3000 μm. The filters are fabricated from thin metal foil with holes. Configuration of the holes depends on the required wavelength.

The filters settle the problems of quasioptical filtration of radiation in THz range. They also permit to get high degree of monochromatization while the aperture ration of device is also high. The Band Pass Filters are highly recommended when it is important to have high spectral resolution with high aperture ratio as well as small overall dimensions and weight of the device.

Applications:

- THz spectroscopy;
- THz testing devices;
- Astronomy, space based astronomy, and astrophysics;
- Materials research;
- Sensors and detectors;
- Electro-optic research.

Features:

- Any pass band in the range from 0.1 to 15 THz (from 3000 to 20 μm);
- High transmittance (60-90%) in pass band;
- Low transmittance (<4%) in stop bands ;
- Available in cryostats and electro-optic assemblies;
- Damage threshold is 65-100 W/cm² (in the range from 0.1 to 15 THz);
- Mounted in holders.

Part Number Designation for Tydex Band Pass Filters: BPF <frequency, THz>-<aperture, mm>

Sizes and Shapes

Round filters with clear aperture/outer diameter 24/31, 35/44, and 47/60 mm and pass band 0.3, 0.5, 1.0, 3.0, 10.0, and 15.0 THz are available from stock. Alternate sizes and custom designs are available upon request.

Transmission Curves

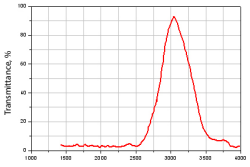

Fig.1 Transmission of BPF0.1

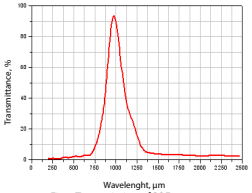

Fig.2 Transmission of BPF0.3

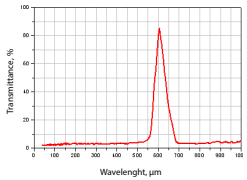

Fig.3 Transmission of BPF0.5

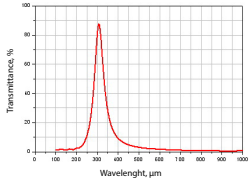

Fig.4 Transmission of BPF1.0

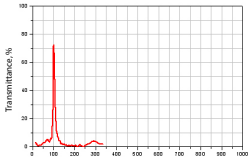

Fig.5 Transmission of BPF3.0

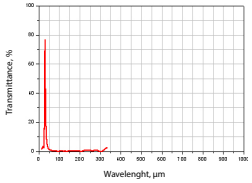

Fig.6 Transmission of BPF10.0

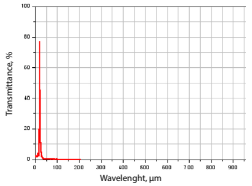

Fig.7 Transmission of BPF15.0

16 Domostroitelnaya str.
194292 St. Petersburg, Russia
www.tydex.ru

Phone: 7-812-3318702
Fax: 7-812-3092958
E-mail: optics@tydex.ru

TYDEX®

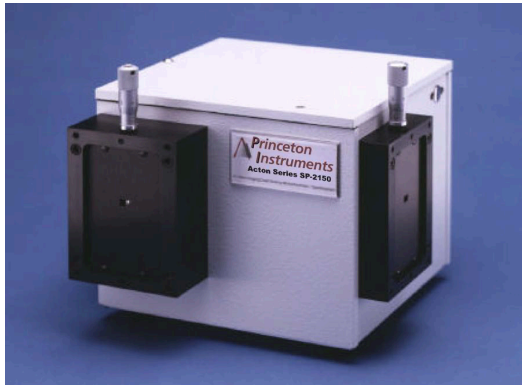

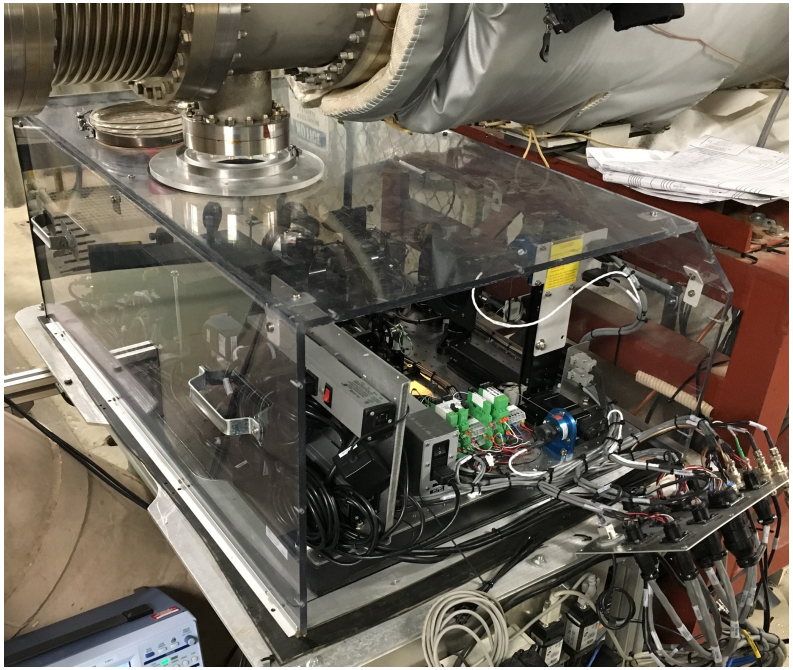

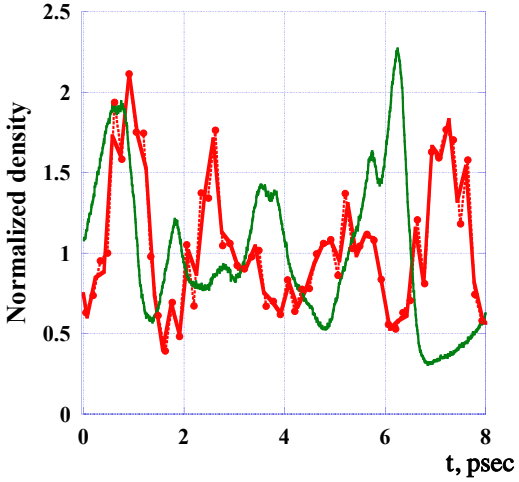
Normalized density
t, psec

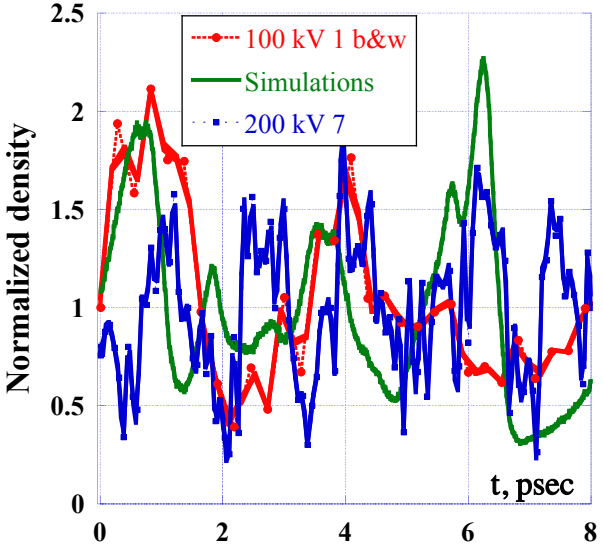
100 kV 1 b&w
Simulations
200 kV 7
Normalized density
t, psec

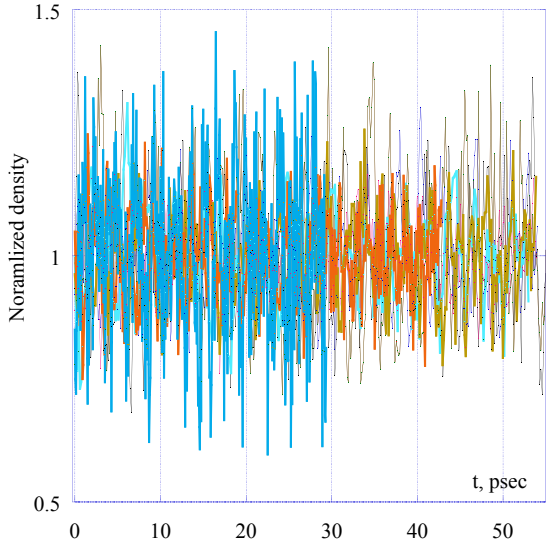
Noramlized density
t, psec

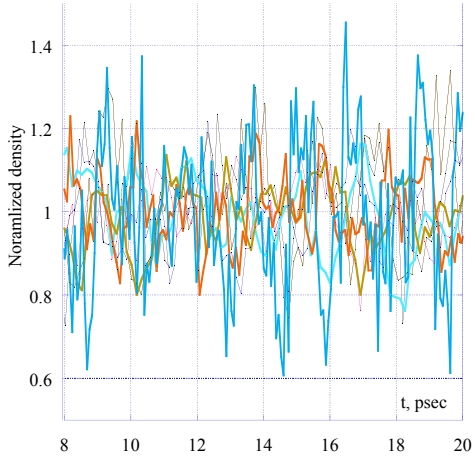
Noramlized density
t, psec

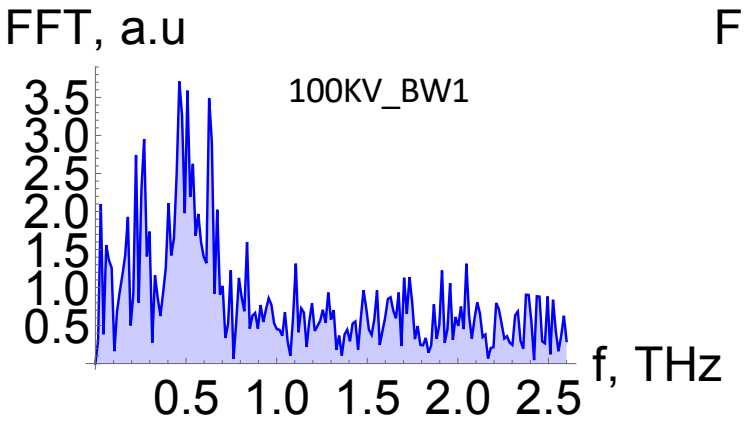
FFT, a.u
100KV_BW1
3.5
3.0
2.5
2.0
1.5
1.0
0.5
0.5 1.0 1.5 2.0 2.5
f, THz

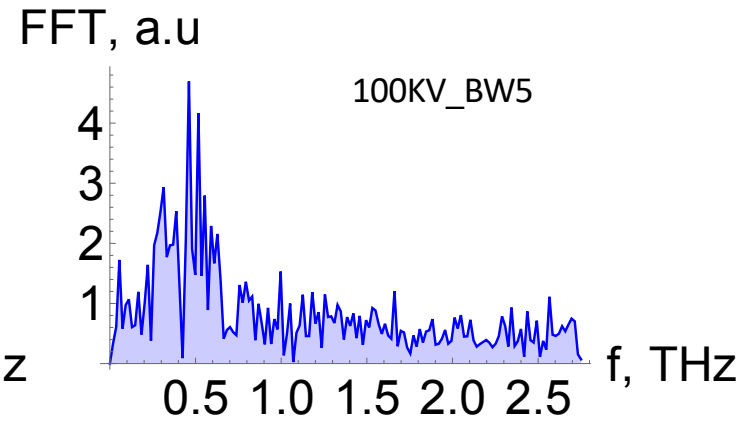
FFT, a.u
100KV_BW5
4
3
2
1
0.5 1.0 1.5 2.0 2.5
f, THz

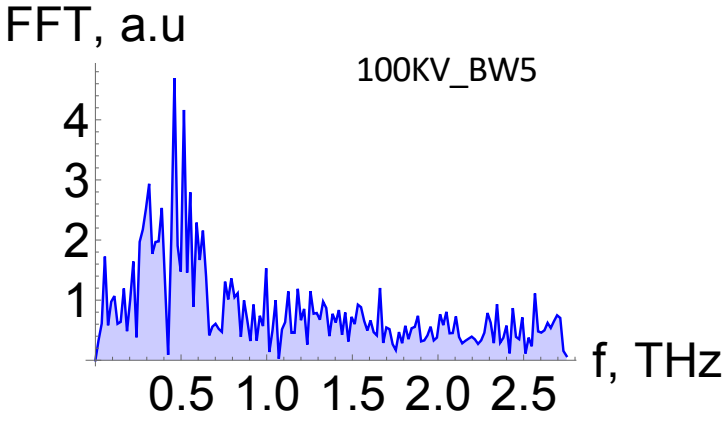
FFT, a.u
100KV_BW5
4
3
2
1
0.5 1.0 1.5 2.0 2.5
f, THz

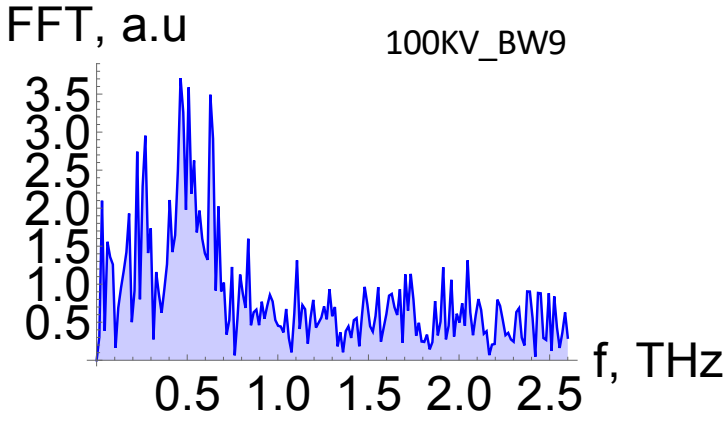
FFT, a.u
100KV_BW9
3.5
3.0
2.5
2.0
1.5
1.0
0.5
0.5 1.0 1.5 2.0 2.5
f, THz

CeC Drive Laser Overview

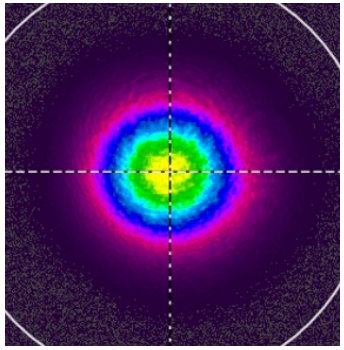

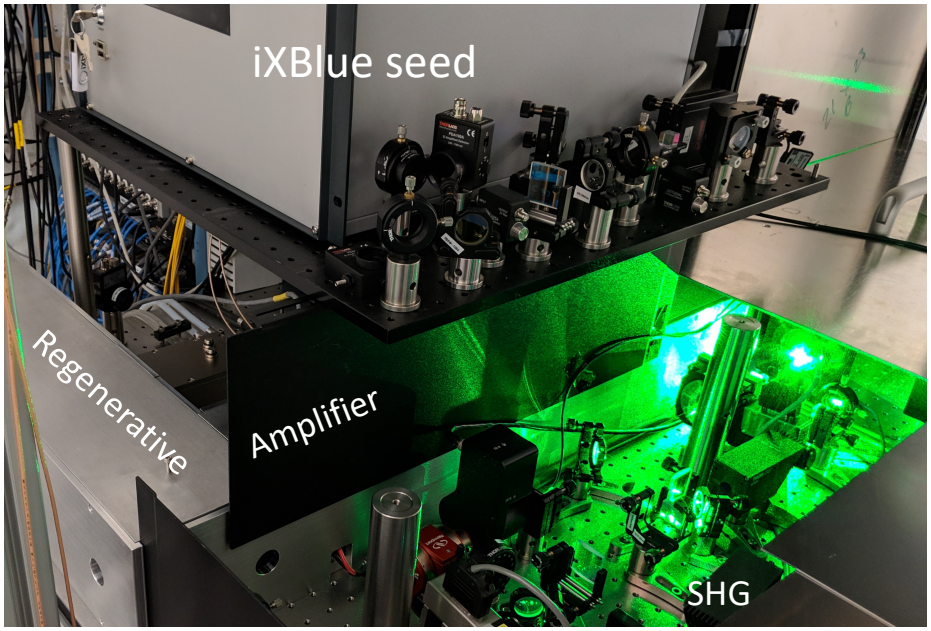

60min Shot to Shot stability **<1.2%** rms (IR)

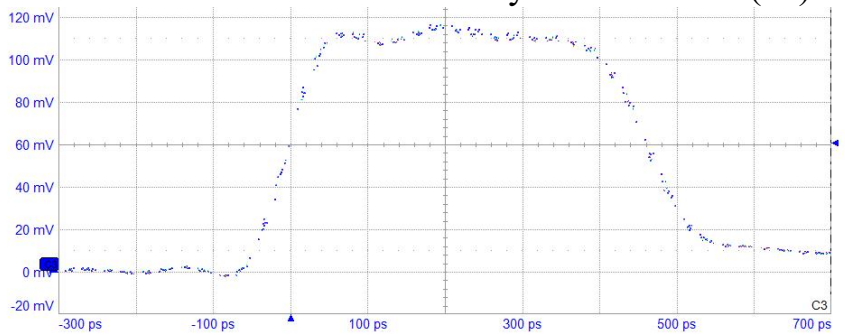

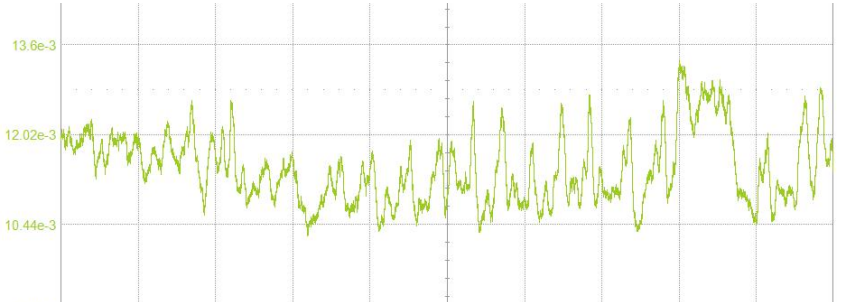

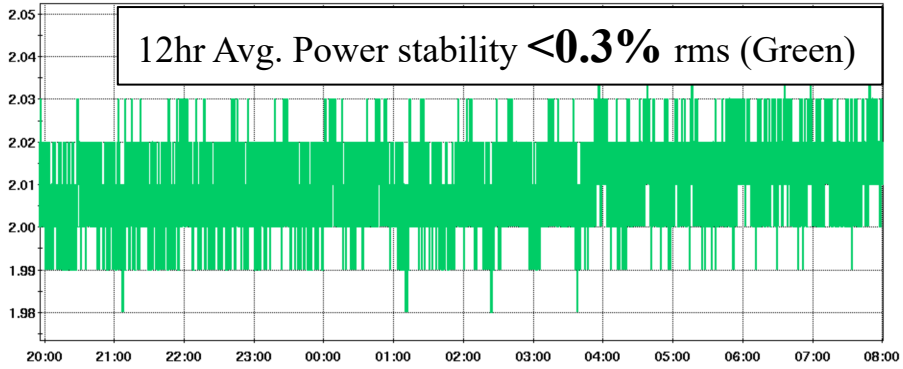

new iXBlue Seed Laser and Pulse Shaper
- 8Gs/sec, 12bit Arbitrary Pulse shape Generation
- Low noise, 10µW avg. power seed

Regenerative Amplifier
- Low noise, high gain amplification (60dB)
- Insensitive to environmental conditions
- 10W Avg. Power output

FEL amplifier and Infrared Diagnostics were fully operational

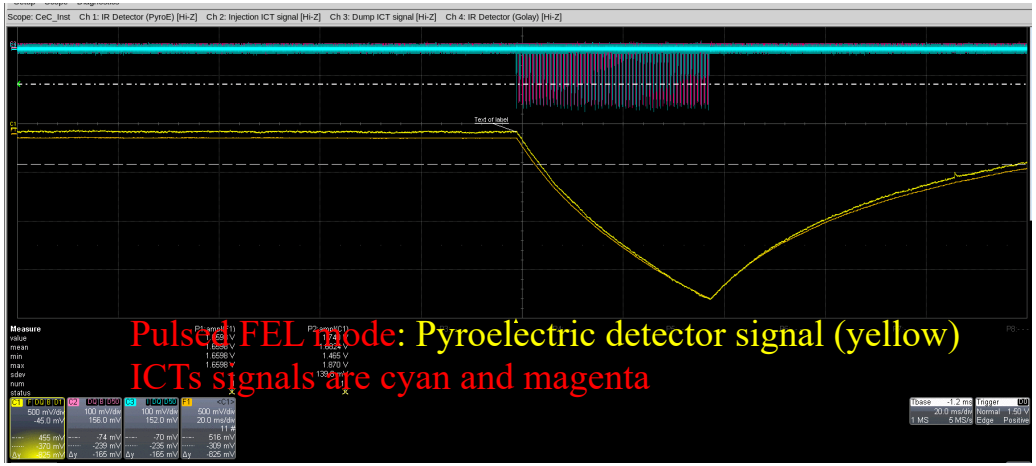

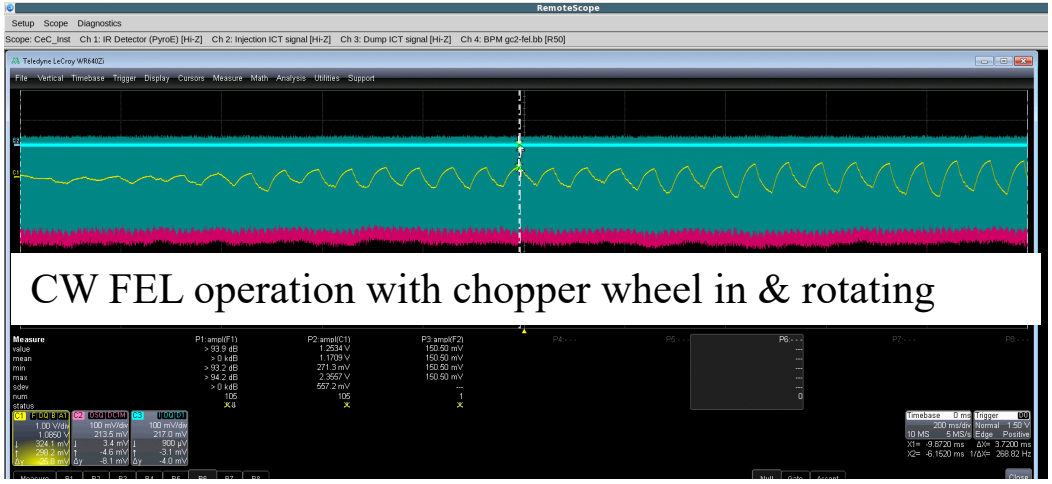

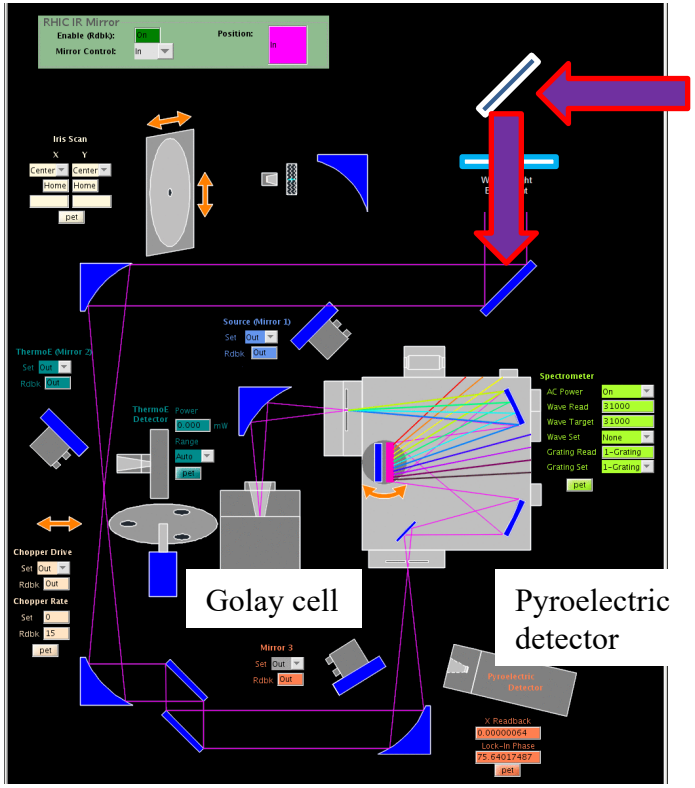

IR diagnostics controls

Run 18 Drive Laser

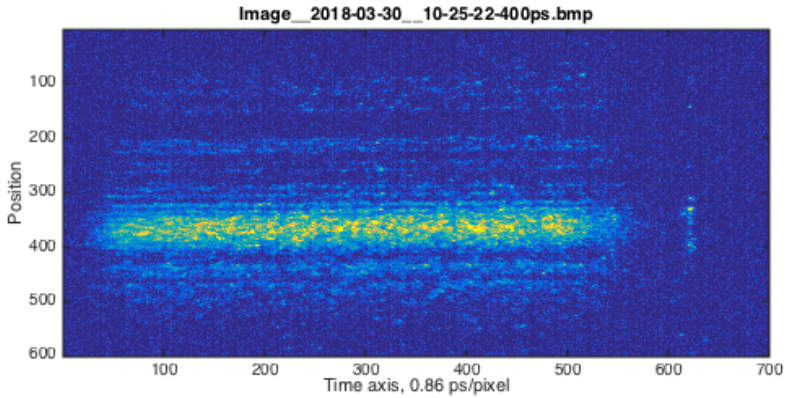

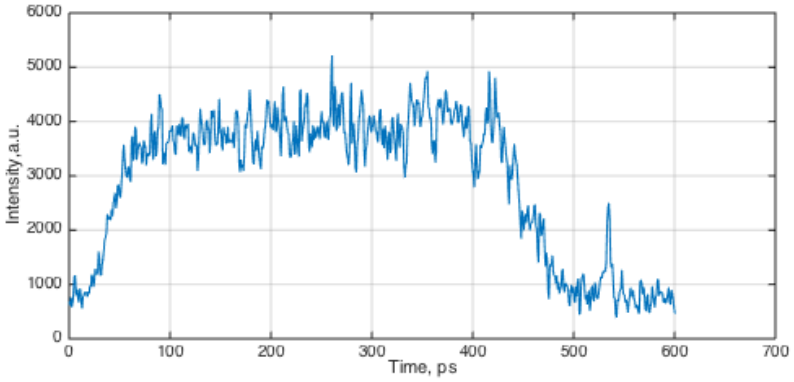

400 psec laser power profile after tuning

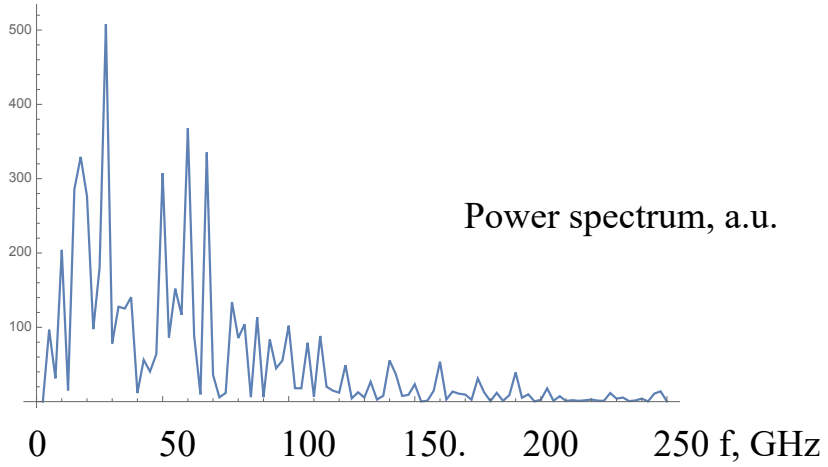

It was found that fiber amplifier induces power fluctuations in the temporal profile as well as shot-to-shot variations. For this reason it was replaced with regenerative amplifier which provided flat top and substantial margin on the laser power to extend cathode lifetime.

The laser trigger set-up was modified to meet the specifications on jitter.

Measured CeC laser spectrum